UNIVERSITAT POLITÈCNICA DE CATALUNYA BARCELONATECH

Microfluidic platform for multiple parameters readouts in a point-of-care

Shadi Karimi

Microfluidic Platform for Multiple Parameters Readouts in a Point-of-care

Autor

Shadi Karimi

Supervisors

Dr. Jasmina Casals-Terré

Dr. Josep Farré Lladós

Escola Superior d'Enginyeries Industrial, Aeroespacial i Audiovisual de Terrassa

Universitat Politècnica de Catalunya

In Partial Fulfillment of the Requirements for the Degree of Doctor by UPC

February 2020

Abstract

The global microfluidics market was valued at USD 4.75 billion in 2018 and it is estimated to be valued at USD 27.90 billion in 2023 [1]. One of the important factors, propelling the growth of the market is the rising demand for Point-of-Care (POC) testing. Microfluidic devices are key in fulfilling this demand due to their portability, small volume of sample requirement, and microfabrication techniques that simplify the industrialization. POC testing not only allows healthcare experts to determine a diagnosis at a patient's bedside, but also empowers non-expert users to observe their health status. One of the most important samples that are used for these microfluidic devices is blood, due to the presence of various biomarkers in it. However, the existence of millions of cells in the blood introduces a great level of noise for the detection the particular biomarkers, therefore, blood plasma separation is the first step for POC blood testing devices.

In this thesis, the design, development, and validation of a POC platform that integrates a novel blood plasma separator (BPS) design to multiple readouts systems is the main goal. To achieve this, firstly, the hypothesis that air bubbles trapped in dead-end zones of a passive BPS can be used to enhance the extraction of plasma from whole blood is validated numerically by the Computational Fluid Mechanics (CFD) and experimentally. According to the results, the proposed design that produces enough quantity and quality of plasma is introduced for the first time in novel forward and reverse ABO/Rh blood grouping POC.

In some other practical situations, there is a need to separate the cellular components from the blood continuously. Therefore, the hypothesis that cross-flow filtration could be applied to separate plasma from blood continuously was investigated. Compared to recent works in the literature [2-7] the proposed device's contribution is capable to optimize either purity or yield of the extracted plasma by calibrating the suitable flow rate depending on the demand of the separation. One of the applications where these characteristics are desirable is in bleeding or thrombotic disorders. Currently, the stressful lifestyle and the aging of the population have led to an increase in such disorders [8,9]. The possibility of having a portable system to evaluate the

global hemostasis of a patient is of great interest to reduce the burden on the public health systems. The proposed BPS was coupled to an interchangeable biomimetic surface to study effects of the new oral anticoagulant Apixaban (APIX) and compare the results to previous conventional techniques. The test showed an excellent agreement with the conventional techniques, while the amount of the required sample and reagent have been reduced.

The prototypes of all the proposed devices were initially fabricated using soft-lithography and wet-etching processes. The scalability of these processes is complex and nowadays machining process based on femtoseconds laser pulses is an interesting candidate for the scalability of the production. Hence, the hypothesis that a novel production method based on direct laser microfabrication method using a femtosecond laser was proven capable to machine the sub-micron channels required for the production of successful BPS. The promising results proved that this method provides a fast manufacturing approach useful for various applications such as POC devices.

Keywords: Separation science, Microfluidics, Lab-on-a-Chip, Point-of-Care, Microfabrication, Blood typing, Hemostasis, high-throughput separation, Capillary separation.

Acknowledgement

Firstly, I would like to express my sincere gratitude to the director of this dissertation, Dr. Jasmina Casals-Terré for the unconditional support throughout my Ph.D. studies and related research. Her endless patience, enthusiasm, motivation, and tremendous knowledge did not go unnoticed, in fact, they helped mold me into the student I am today. Dr. Casals-Terré was the primary resource for my science questions. I am also thankful for the co-director of this dissertation, Dr. Josep Farre Llados for his continuous support of my Ph.D. and helpful guidance at the laboratory. His kindness, discipline and perfectionism, paved the way of my research plan.

I am very grateful to be in the Mechanical department of UPC under the management of Prof. Jordi Romeu Garbi, who is one of the kindest individuals I have ever come across. It was under his warm support that I was able to successfully overcome any difficulties as well as learn from them. I am also very grateful to Dr. Mohammad Mojaddam, Dr. Gines Escolar Albaladejo and Dr. Enrique Mir for their interest in this project and for their continuous support and advise which helped me through my career.

I would like to thank all the members of the Microtech lab for all the discussions we would have and for their helpful suggestions and comments during our weekly meetings. I would like to thank Pouya in particular, my officemate for more than four years who was always there to help me solve any problems that arose. Thanks to Dr. Mehdi Mohammadi and Dr. Hojjat Madadi for helping me without any hesitation despite their overwhelmingly busy schedule.Thank you to all my friends who helped me overcome the living abroad challenges all while making it an enjoyable experience for me.

Special acknowledgments to SENSOFAR's CEO Prof. Ferran Laguarta, Microrelleus company in Sabadell, Hospital clinic of Barcelona, Mutua of Terrassa, and Eurecat company in Cerdanyola del Vallès.

Now onto my boyfriend, Hooman. Hooman has been an incredibly great supporter during both my good and bad times. The past years have not been easy to say the least, I mean that both academically and personally; and for that I sincerely thank him for sticking by my side through the ups and downs; even when I was overwhelmed and in turn irritable.

Finally, I want to express my deepest gratitude to my parents and siblings without whom I would never have enjoyed so many opportunities and I would not have had the courage to begin this adventure in the first place. Thank you for believing in me and encouraging me to follow my dreams.

Cheers to new adventures.

Abbreviations

APIX	Apixaban
BPS	Blood Plasma Separator
CSF	Cerebrospinal Fluid
CFD	Computational Fluid Dynamic
CFL	Cell-Free-Layer
CTC	Circulating Tumor Cells
DOAC	Direct Oral Anticoagulant
ELISA	Enzyme-Linked Immunosorbent Assay
HPR	High on-treatment Platelet Reactivity
IR	Infrared
LOC	Lab on a Chip
LPR	Low on-treatment Platelet Reactivity
MTB	Mycobacterium Tuberculosis
PBCT	Pre-transfusion Bedside Compatibility
PDMS	Polydimethylsiloxane
POC	Point-of-Care
POCT	Point-of-Care-Testing
PPP	Plasma Poor in Platelets
PRP	Plasma Rich in Platelets
PT/INR	Prothrombin Time and International Normalized Ratio
RBC	Red Blood Cell
VKA	Vitamin K Antagonists
WBC	White Blood Cell

List of publications

This thesis is based on the following articles, which will be referred to by their roman numerals in the text.

I. Shadi Karimi, Pouya Mehrdel, Josep Farre Llados, Jasmina Casals, A passive portable microfluidic blood-plasma separator for simultaneous determination of direct and indirect ABO/Rh blood typing, Lab on a chip Journal, 2019.
(*https://doi.org/10.1039/C9LC00690G*)

II. Shadi Karimi, Josep Farré Llados, Enrique Mir, Ginés Escolar, Jasmina Casals-Terré Hemostasis-On-Chip: Impedance spectroscopy meets microfluidics for hemostasis evaluation, Micromachines, 2019.
(*https://doi.org/10.3390/mi10080534*)

III. Shadi Karimi, Pouya Mehrdel, Josep Farre Llados, Jasmina Casals, Rapid and cost-effective laser direct microfabrication of sub-micron depth, Biofabrication Journal, 2019.
(*https://doi.org/10.1088/1758-5090/ab6665*)

IV. Shadi Karimi, Mohammad Mojaddam, Sahand Majidi, Pouya Mehrdel, Josep Farre Llados, Jasmina Casals, Optimization of a high throughput blood plasma separator via 3-D simulation and experimental testing, submitted to Lab on a chip Journal, 2019.

Contents

Overall objectives

The general goal of this thesis was to design and develop microfluidic BPS that could contribute to the construction of future lab-on-a-chip (LOC) systems, especially for POC applications. Microfluidics is the science of controlling and manipulating fluids, usually in microliters range, inside the microchannels. This technology has started in the early 1990s and has grown exponentially [10]. It is observed that microfluidics is an essential tool for life science research or from a larger point of view in biotechnologies.

Based on the aforementioned hypothesis the more specific goals were:

1. To validate that air bubbles trapped in dead-end zones of a passive BPS can be used to enhance the extraction of plasma from whole blood providing a higher yield.
2. To design and fabricate a portable ABO/Rh blood typing test that performs both direct and indirect methods simultaneously from a single blood droplet by integrating the optimized BPS with the required biomarkers.
3. To validate the possibility of utilizing the cross-flow filtration for continuous plasma extraction from the blood by optimizing the BPS dimensions and geometric design, numerically and experimentally.
4. To design and fabricate a hemostasis-on-a-chip platform to evaluate hemostasis disorders near the patients by combining the BPS and impedance spectroscopy techniques.
5. To define a manufacturing methodology that uses infrared (IR) ultrashort pulse direct laser also known as femtoseconds laser microfabrication method to batch manufacture the aforementioned designs.

The various studies included in the thesis deal with the need of a microfluidic BPS that can be integrated with multiple parameters readouts to make POC systems Figure 1 shows a current integration of the BPS with a lateral flow test strip, which is currently in process of commercialization.

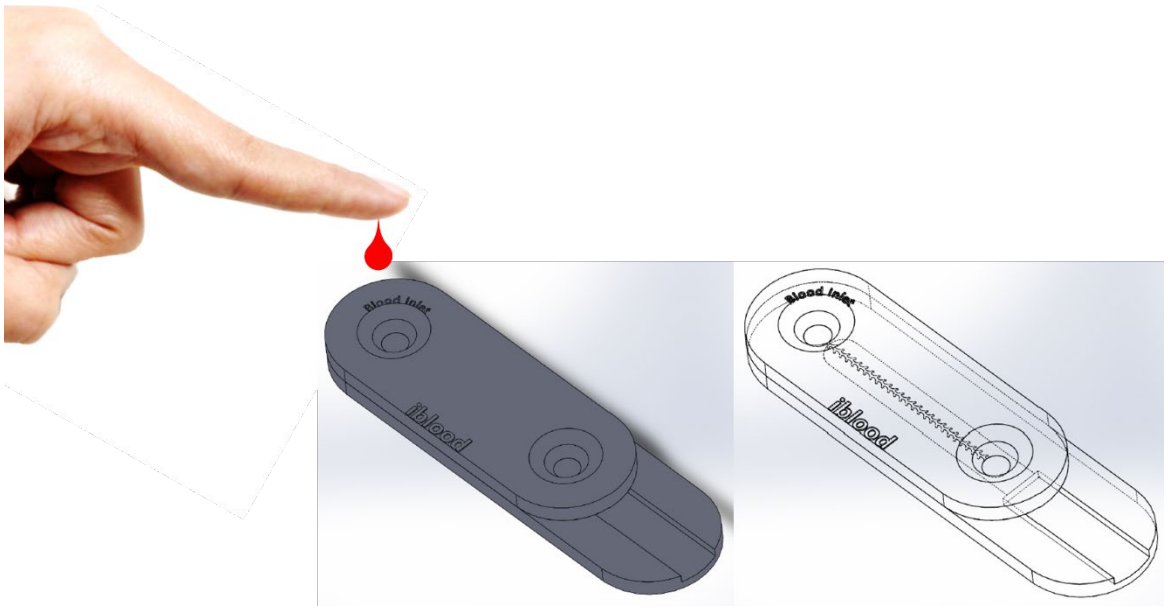

Figure 1. Schematic picture of the microfluidic BPS design in progress to be in the market.

Introduction

Human blood

Blood is the most important body fluid in clinical diagnosis and it is also one of the simplest ways to determine the internal performance of the human body studying its cellular components, such as red blood cells (RBC), white blood cells (WBC), platelets and the rest of the biomarkers suspended in the plasma (Figure 2a). Researchers have characterized the rheological behavior of blood, estimating a density of $1060\ kg/m^3$ and a viscosity of $0.02\ Pa.s$[11].

RBCs occupies around 44% volume in the blood, typically shaped as biconcave discs (Figure 2b) approximately 6 to 8 µm in diameter and a thickness at the thickest point of 2 to 2.5 µm and a minimum thickness in the center of 0.8 to 1 µm. Being very elastic and much smaller than most of the other human cells, under high shear flows the shape of the red blood cells can deform reducing its smaller dimension even to less than 1µm. WBCs are approximately 1% of blood volume and are spherical cells with approximately 8.5 µm in diameter and they defend the body against infection. Platelets make up a blood volume of approximately 0.7% and are responsible for blood clotting in the case of an open wound. Platelets have a discoidal shape; they are approximately 2 to 4µm in diameter and 1 µm in thickness and are much stiffer than RBCs. These blood cells are suspended in the liquid phase of blood (Plasma), which is straw-yellow in color and occupies approximately 54% volume in the blood. Plasma is essentially an aqueous solution with various circulating biomarkers such as antibodies, hormones, nutrients, the end-products of cellular metabolism, clotting factors, immunoglobulins and an abundance of proteins [12,13].

Biomarkers indicate the presence of certain diseases in an individual, therefore, plasma is the base of a wide range of assays and is needed at clinical chemistry testing for prognosis and clinical diagnosis of diseases [14]. Existence of the blood cells in plasma may provide a great level of noise in the biochemical determinations and reduces or interferes the precision of different sensing technologies during the analysis, therefore, cell separation from plasma is one of the most basic, essential steps in disease diagnostics field and it is a major challenge since more than 5 million cells have to be separated from one microliter of blood [15].

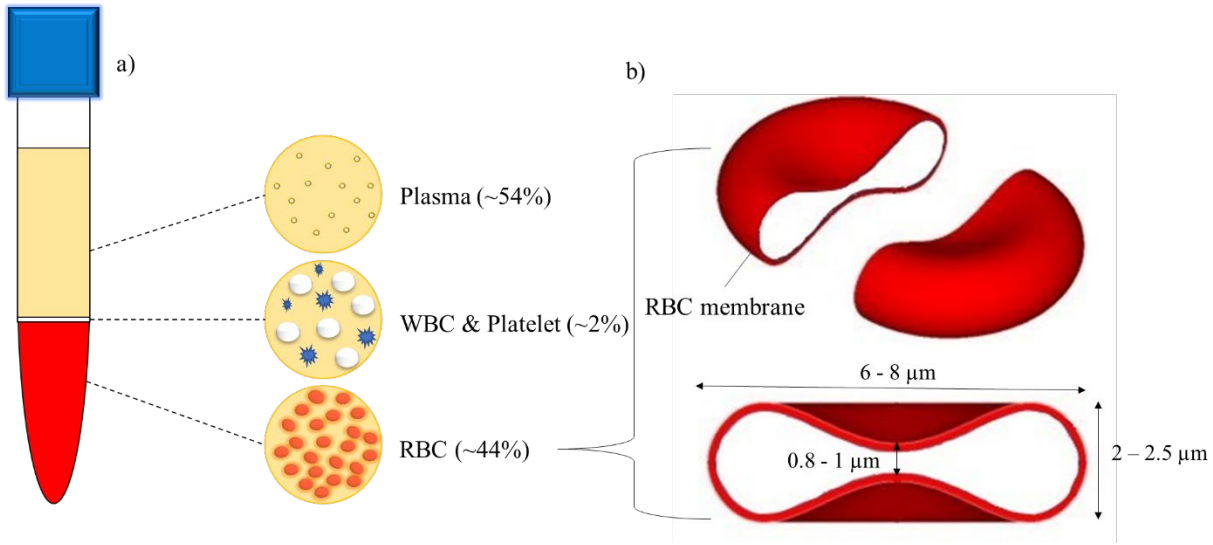

Figure 2. a) The schematic pictures of the blood components, b) Three-dimensional cross-section of a single RBC with its dimensions.

Filtration

There are definitely different situations where separation is a key step. For instance, clinical analysis, diagnosis, and preparation techniques rely heavily on separation at some stage of the process. Since many biologically relevant samples such as whole blood, saliva, and cell lysates are highly complex and because the targets for detection can be present in extremely low concentrations, separation is often an essential part of any analytical process. In lab environments, centrifugation is generally accepted as the most conventional method. Although the process of centrifugation is easy and widely employed, it limits its usage to a laboratory. Therefore, some of the drawbacks associated to this process are the large volume of sample requirement, the increased number of manipulation errors, its bulkiness, the required time to process the sample and in some cases it may result in rupture of blood cells due to the centrifugal force [16].

The needs for miniaturization

Employing microfluidic devices have been considered as an effective manner to overcome many of the aforementioned limitations, providing the same effectiveness with smaller volume

requirement of the blood sample. The introduction of microfabricated BPS allowed preanalytical standardization, cost-effectiveness, rapid measurements, portability, protection against contamination and evaporation, the advantage of working with the laminar flow which allows controlled mixing, and decreased reagent consumption. Besides, the microfluidic blood/plasma separation methods have the advantage of connecting directly to microsensors and creating miniaturized diagnostic devices.

The aforementioned advantages, not only empower the chronic patient having a portable diagnostic tool to monitor their health status, but also can help the undeveloped countries, to have access to the best medical diagnostic technologies. Microfluidic systems allow miniaturization and integration of complex functions, which could move sophisticated diagnostic tools out of the developed-world laboratories. These systems must be inexpensive, accurate, reliable, rugged and well suited to the medical and social contexts of the developing world [17].

In recent years, considerable progress is made in the development of microfabricated systems for its use in the chemical and biological sciences. The development has been driven by a need to perform rapid measurements on a small volume of sample. However, at a more primary level, interest in miniaturized analytical systems has been stimulated by the fact that physical processes can be more easily controlled and harnessed when instrumental dimensions are reduced to the micrometer scale. Such systems define new operational paradigms and provide predictions about how molecular synthesis which might be revolutionized in the fields of high-throughput synthesis and chemical production [18].

POC testing devices

As it is mentioned previously, the overall objective of this research is developing a stand-alone POC device which can implement different types of tests without the need for sample pretreatment to diagnose the patient's disease with high efficiency at a reasonable time (minutes at most). The goal for many researchers in the fields of microfluidics and LOC is the development of devices that will be able to diagnose a patient on the spot, wherever the patient happens to be, in just a few minutes without the need for extensive laboratory testing.

POC diagnostics or bedside tests are medical tools or devices that can diagnose disease in a patient's community, outside of a hospital setting. They include both low-tech and high-tech. The

driving notion behind a point-of-care-test (POCT) is to bring the test conveniently and immediately to the patient. This increases the likelihood that the patient, physician, and care team will receive the results quicker, which allows for immediate clinical management decisions to be made.

In recent years the use of POCT has been spread and some biomarkers are commonly being determined by POCT devices such as blood glucose testing, rapid coagulation testing (PT/INR), rapid cardiac markers diagnostics (TRIAGE), drugs of abuse screening, urine strips testing, pregnancy testing, fecal occult blood analysis, food pathogens screening, hemoglobin diagnostics (HemoCue), infectious disease testing and cholesterol screening glucose, blood gas analysis/electrolytes, activated clotting time for high dose heparin monitoring, and rapid strep [19].

Miniaturized blood plasma separation technique has been thriving from 2006. Most POC systems need microscale blood plasma separation [20]. Plasma from blood has to be extracted in order to proceed with most tests. A variety of solutions has appeared recently to miniaturize blood plasma separation, which has currently been performed in three main formats [21]:

1. The **CD format** is based on a radial geometry and exploiting the laser CD developments (Figure 3a). The CD-based format allows neat sample preparation as well as analysis, and therefore, are good examples of LOC devices in terms of functional integration. An excellent exhaustive review of the subject [22,23] showed that the plasma extraction in a CD-based format relies on the centrifugal force forcing the heavy cellular content towards the external edge of the CD, while the plasma is siphoned out by various valving systems. The success of the plasma separation in CD format relies on these valving systems, which have included passive siphoning, [24] hydrophobic, capillary, [25,26] or ferrowax microvalves [2827,28]. Protocols on the CD-based format are rapid, and the fabrication of CD cartridges is simple and cost-effective. Parallelization is enabled by having several similar chambers within one CD cartridge. However, the technology is limited by the use of numerous valves and the fact that the movement of fluid from one chamber to another relies only on the centrifugation speed [22].

2. The **paper format** is based on capillary flow migration on a cost-effective and biodegradable resource (Figure 3b). From 2009 paper-based microfluidics has been the center of a flurry of research activities [29,30]. Paper has been widely used for lateral-flow assays, such as glucose and lipid measurements [31], coagulation measurements [32] or pregnancy tests. But more recently, the paper has been re-engineered to host a variety of integrated microfluidic functions, including plasma extraction from blood. Paper is used in several devices to extract plasma from blood, few examples showcase paper as the only supporting format for the entire assay. While paper can be used conveniently to separate several microliters of blood such as finger-prick volumes, it rapidly clogs and is unsuitable for larger volumes, limiting its use to the analysis of highly concentrated analytes, such as glucose [33] or abundant proteins [34]. However, its low volume of extracted plasma, limits the variety of the applications and it is expected that researchers in the paper field will come up with several analysis techniques compatible with low plasma volume, which might translate into a range of useful commercial lateral flow diagnostic kits.
3. The **microfluidic chip format** is featuring fluid flowing through microchannels and based on classical microfabrication techniques (Figure 3c). Practically, the procedure of blood plasma separation in microfluidic devices can be performed using either passive or active mechanisms. Passive methods work autonomously taking advantage of sedimentation [35-42], microfiltration [43-53], and cell deviation [54-69] while active microfluidic methods rely on external energy sources such as acoustic separation [70-74], electrical forces [75-77], and magnetic separation [78-83]. While paper format only works for passive applications and CD formats only for active applications, microfluidic chip formats can be versatile. This format of blood/plasma separation can be portable, low cost and integrated with continuous-flow separation processes as well. In this thesis, a BPS microfluidic design will be analyzed and optimized to separate by passive and active methods.

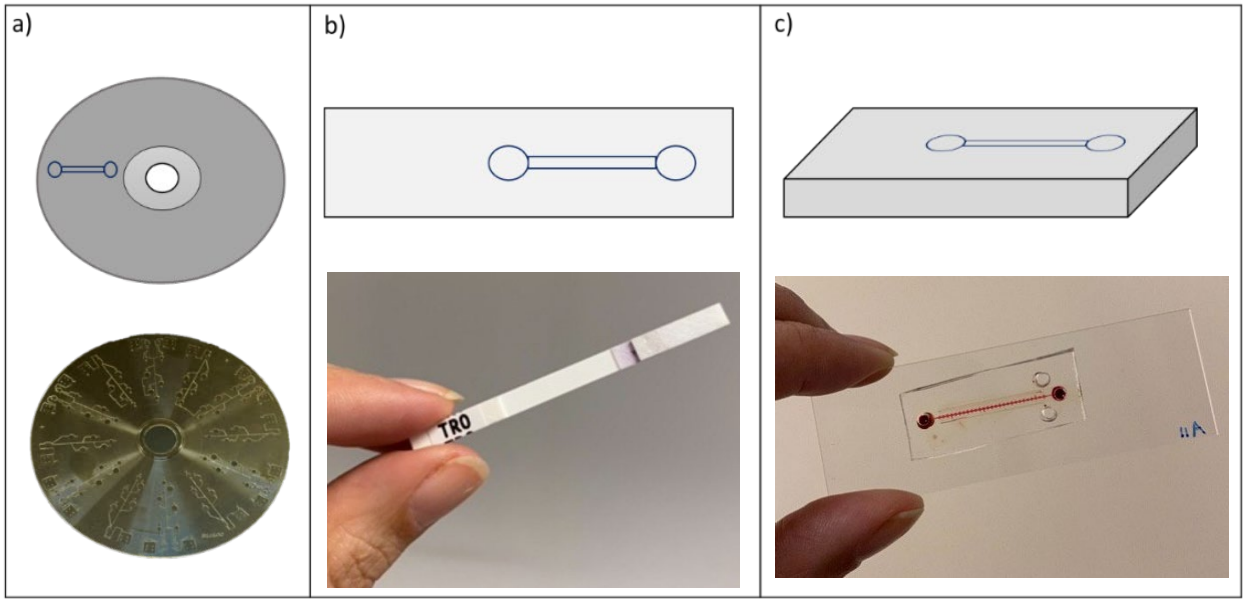

Figure 3. Three different filtration formats. a) CD format, b) Paper format, and c) Microfluidic chip format.

Methods

Passive

Passive separation methods refer to those that not using external forces relay on the channel geometry and the capacity of the particles/cells to diffuse, intrinsic hydrodynamic forces, such as punch flow fraction, deterministic lateral displacement, inertial forces and intrinsic physical property of the cells such as sedimentation to induce plasma extraction from cell components. In these separation methods, particles are sorted exclusively by their mechanical properties, such as size, shape, and deformability, using only the geometries of microchannels, the flow itself, and inherent hydrodynamic forces.

Blood plasma separation from undiluted blood without the help of external forces is essential to create a POC device. Most of these passive techniques suffered from clogging problems and low yield [84,85]. This issue limits the amount of plasma available for analysis and consequently the type of test that can be implemented using microchip filtration. Therefore, the main challenge in the passive method is postponing the clogging process and achieving a higher yield.

Active

Active separation refers to the defined manipulation of the working fluid by active components such as micropumps, microvalves or other external forces such as electric, acoustic or magnetic. Continuous-flow separation using microfluidics devices enables the separation of a fluid by an external imposed flow rate generate by micro-pump through microchannels that deviates particles trajectory through hydrodynamics. However, their low-throughput or low separation efficiency is preventing the adoption of this technology for continuous-flow separation [2,3,5,86,87]. Continuous-flow processes are used in a wide range of applications such as bioanalytical, chemical, energy and environmental fields [88].

The physics of blood flow

Blood is a complex, and multicomponent fluid; therefore, the modeling and analytical prediction of its flow behavior is a challenge. Blood flow in the body is generally considered as laminar flow

and from a physical point of view, can be defined as a non-Newtonian, and shear-thinning fluid due to its cellular suspension.

The margination of particles in blood has applications in microfluidic devices for the removal of pathogens and also for the separation of cells. It is, therefore, vital to understand the mechanisms that are responsible for margination. For margination to occur, the particles need to escape the fluid-flow streamlines and move laterally as a result of gravity, buoyancy, hydrodynamic forces, van der Waals forces, and/or Brownian motion. The trend is resulted from the competition between the adhesion to the walls and drag forces. At low shear rates, the adhesion forces are larger than the drag forces, regardless of the particle orientation. At higher shear rates, these forces depend on the orientation of the particle [89].

The forces exerted on a cell in a microfluidic channel are lift force, drag force induced by lateral fluid flow, buoyant force, and gravitational force which are shown in Figure 4. The net force acting on a cell can be expressed as:

$$\vec{F}_{net} = \vec{F}_L + \vec{F}_D + \vec{F}_B + \vec{F}_g \qquad 1$$

Where $\vec{F}_L$ is the lift force in Y direction (width of the channel), $\vec{F}_D$ is the drag force in X direction (length of the channel), $\vec{F}_B$ is the buoyant force in Z direction (height of the channel) and $\vec{F}_g$ is the gravitational force in Z direction (height of the channel). Gravity facilitates the migration of the larger particles (500 nm to 10 μm) in the direction of the gravitational force.

In a microfluidic channel, because the Reynolds number is typically low, the drag force also known as Stokes's drag can be expressed as follows:

$$F_D = -6\pi\mu R(v_m - v_p) \qquad 2$$

where R is the radius of the particle, μ is the viscosity of the medium, v_m is the velocity of the flow, and v_p is the velocity of the particle. The buoyant force acting on a spherical particle suspended in a medium can be expressed as follows:

$$F_B = {}^4/_3 \pi R^3 \rho_m g \qquad 3$$

where ρ_m is the density of the medium, and g is the acceleration due to gravity. The gravitational force acting on a spherical particle is expressed as follows:

$$F_g = {}^4/_3 \pi R^3 \rho_P g \qquad 4$$

Where ρ_P is the density of the particle. The gravitational and buoyant forces only act in the vertical direction on the cell, whereas the drag force acts in the lateral direction. In human blood, the density of the plasma (1.025 g/ml) is smaller than that of the RBCs (1.097 g/ml), WBCs (1.073 g/ml), and platelets (1.045 g/ml). Thus, all the blood cells sink as they follow the flow in the microfluidic channel [87].

The lift force leads to migration across the streamlines. In the expansion structure of the microchannel where the streamline changes direction smoothly, a particle is primarily subjected to the shear-gradient lift force ($\vec{F}_{L_s}$). As it is shown in Figure 4, it is arising from the curvature of the Hagen-Poiseuille flow that acts downward and parallel to the velocity gradient and drives the particle towards the channel walls. On the other hand, the wall-effect lift force ($\vec{F}_{L_w}$), that acts upward and parallel to the velocity gradient, pushes the particle away from the wall toward the channel centerline; the net force of these two forces is the lift force ($\vec{F}_L$) that is responsible for particle migration away from the wall.

This lift force can be calculated by:

$$F_L = \mu\dot{\gamma} \frac{r^3}{h} f(1-v) \qquad 5$$

Where $\dot{\gamma}$ is the shear rate, r is the radius of the particle, h is the particle's distance from the wall and $f(1-v)$ is a dimensionless function based on the reduced particle volume and is given by:

$$V = \frac{v}{\frac{4}{3}\pi(\frac{S}{4\pi})^{3/2}} \qquad 6$$

where V is the enclosed volume and S is the surface area of the particle [89].

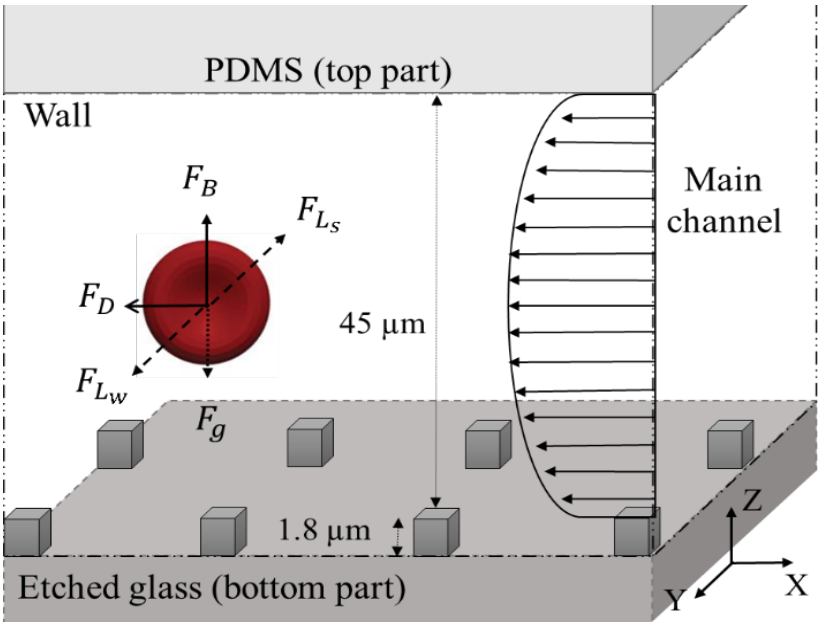

Figure 4. The schematic of side view of the micro channel. The forces exerted on the cells in a microchannel. $\boldsymbol{F_{L_s}}$ is the shear gradiant lift force and $\boldsymbol{F_{L_w}}$ is the wall induced lift force and $\boldsymbol{F_L}$ is the net lift force, $\boldsymbol{F_D}$ is the drag force, $\boldsymbol{F_B}$ is the buoyant force and $\boldsymbol{F_g}$ is the gravitational force.

Generally, the discoidal shape of RBCs, combined with their elasticity and membrane fluidity, results in strong lift forces that push RBCs toward the center of the channel and lead to the formation of a CFL.

The microfluidic channels with large aspect ratio cross-sections are largely influenced by channel geometry, particle size, and flow properties changes. The CFL thickness varies with the channel diameter and its geometry. The CFL layer is thicker for higher flow rates, since the lift force pushes particles stronger away from the walls [92].

The principle of design

The proposed BPS design is taking advantage of several aspects including hydrodynamics, and blood rheology in order to maximize the volume of extracted plasma. As it is depicted in Figure 5a, this design contains two parts: the top part which has three separated microchannels; one main

channel for the passage of blood and two side channels also known as plasma collector channels which are responsible to collect the plasma flowing from the sides of the channel due to the axial migration effect of the red blood cells across the main channel. This part is fabricated using the conventional soft-lithography technique on a single layer of polydimethylsiloxane (PDMS). The bottom part is a tank placed below these microchannels for plasma collection, which is fabricated via the wet-etching method on a glass substrate. This tank contains an array of pillars to hold the weight of the PDMS and create a capillary pump that fosters the plasma separation. The plasma in the tank will be collected by capillary force via two plasma collector channels as it is illustrated in Figure 5b. The pillars are chosen to be in a diamond shape, since they have minimum fluidic resistance compared to other shapes such as circle, elongated, pine and rectangular [90]. The depth of the tank is selected to be below 1.8µm which is less than the minimum size of RBCs, therefore,

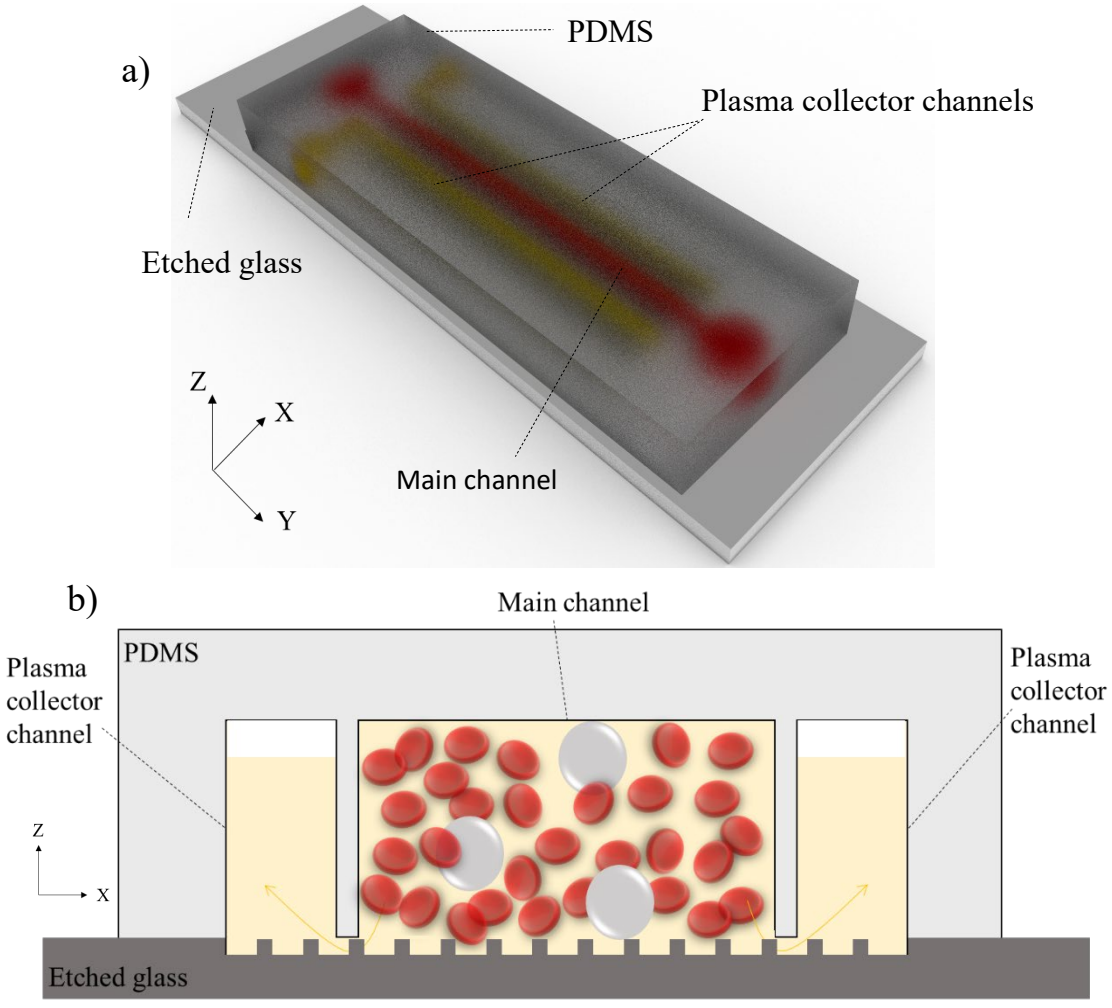

Figure 5. a) Schematic picture of the complete BPS device, b) The cross-section view of the BPS device.

blood cells cannot penetrate from the main channel to the plasma collector channels and 100% pure plasma could be extracted from the whole blood.

The initial design of the main channel [90] as it showed in Figure 5 was a simple straight channel. This previous passive design obtained a yield of 2% from the whole blood and to increase the yield the active separation techniques such as dielectrophoretic forces were helped to separate 10% plasma from diluted blood (1:1). Therefore, in this work, the goal was to improve the yield for both passive and active methods from undiluted blood. The results from the previous designs are tabulated in Table 1. The yield and purity of the extracted plasma were calculated by these equations:

Table 1. The comparison of the previous designs based on the yield and purity of the extracted plasma.

	Method	**Design**	**Dilution ratio**	**Yield**	**Purity**
Madadi et al. [46,90]	Passive	Straight	No	2%	98%
Mohammadi et al. 76]	Active	Corrugated	1:1	10%	99%
Mohammadi et al. [77]	Active	Straight	1:1	10%	>99%

$$\text{Yield} = \left(\frac{\text{output sample volume}}{\text{input sample volume}}\right) * 100 \qquad 7$$

$$\text{Purity} = \left(1 - \left(\frac{\text{final cells density}}{\text{initial cells density}}\right)\right) * 100 \qquad 8$$

According to Fåhræus–Lindqvist effect [91] the viscosity of the blood, changes with the diameter of the tube it travels through. For the tubes with the diameters between 10 to 300 µm, the cells will travel in centerline and near the main channel's wall a layer free of cells will form known as cell-free-layer (CFL) which facilitate the extraction of plasma. Therefore, a longer perimeter of the main channel´s walls should lead to the release of more plasma. On the other hand, the appearance of a dead-end zone due to hydrodynamics [76] showed that the length of the branches longer than 400 µm highlights RBCs can be captures on these areas slightly diminishing the number of

circulating RBCs. Therefore, in order to take advantage of these effects, the design proposed by Madadi et al. was modified to design 2 as it is depicted in Figure 6. This design has the particularity that at the end of each corrugated channel initially a bubble of air is created and shortly after disappeared due to the PDMS permeability to gasses. The vanishing time of these bubbles is longer than the time required to fill the channel by capillarity, therefore this process acted as an additional pump enhancing the possibility to extract more plasma from the initial droplet. Design number 3 has a larger zone at the end of each branch as it is shown in Figure 6, to enhance the size of the bubble to pull the cells to the side and postpone the clogging process in the main channel. After successfully separating a higher volume of plasma from the whole blood due to the trapping cells in the corrugated channels, compared to the previous devices, design number 4 was proposed. This design has the inclined branches in which the results from CFD simulation showed that it facilitates the RBCs to travel to the sides compared to the perpendicular branches. All of the aforementioned designs were symmetrical and the main channel's width was increased while approaching each of the branches. The CFD models showed that the cells slowed down at the entry of the branches as a result of an increased cross-section of the main channel. Therefore, design number 5 with an asymmetrical characteristic enhanced its predecessors due to an increased velocity of the flow at the main channel compared to the symmetrical designs. By adding an expansion-contraction to this design, as it is illustrated in Figure 6, design 6 was proof to provide the highest yield among the other designs. These constrictions that are created in the main channel, generated a local flow acceleration and delayed the RBCs clogging of the filtration area. The optimized design could postpone the clogging process by the aid of bubble-based lopsided channels, and an expansion-contraction geometry which consequently maximized the volume of the extracted plasma. Therefore, the design for the passive BPS is selected and the second parameter which is the impact of the height of the main channel is studied numerically and experimentally. The results showed that the shorter height leads to extract more plasma. For this reason, the height of 15 µm is fixed for the proposed design. This passive BPS approached 12% yield with 100% purity in approximately 10 minutes. Therefore, an adequate amount of plasma which is needed to perform the ABO/Rh test, is achieved which is explained in detail in Article I.

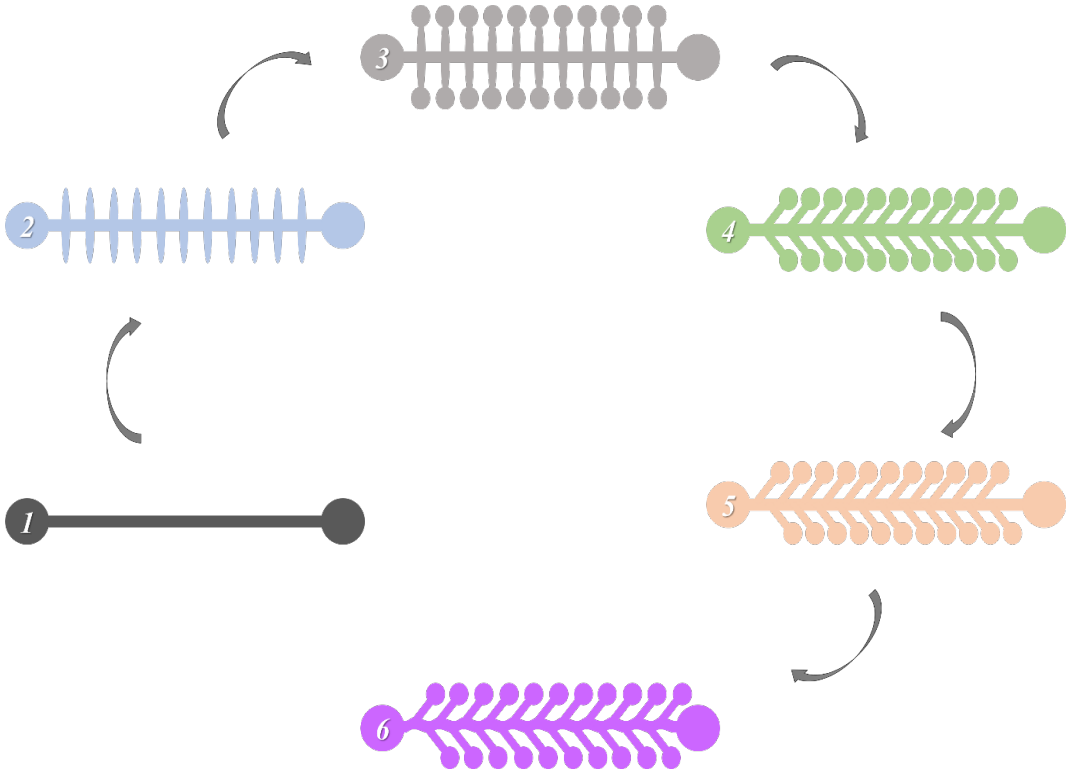

Figure 6. Design development; 1) simple channel, 2) corrugated channel, 3) corrugated channel with the larger zone at the end, 4) lopsided channel, 5) asymmetric lopsided channel, and 6) Final design.

For the active applications by imposing a flow rate, the cells still follow the flow lines due to the channel dimensions (small value of Reynolds number) so that the flow is in the complete laminar zone. Therefore, the cells could not escape to the branches and with flow rates in the range of 1 to 10 $^{mL}/_{h}$ the larger zones at the end of the branches stayed empty. Figure 7 shows the flow path of the corrugated channel for high-throughput applications. The experimental setup of the active BPS is illustrated in Figure 7a, and the real device with the connectors are depicted in Figure 7b. There is a blood inlet which is connected to the syringe pump, one blood outlet, and one plasma outlet which are collected in separate syringes. Figure 7c is the velocity streamline of the 3D simulated BPS in the corrugated channel. The best design for the active method from the numerical results is the one without pillars, which is impossible in practice to deal with due to the flexibility of PDMS that will collapse the channel. Therefore, the idea of replacing the PDMS with another

material which can be rigid, hydrophilic and be fabricated below 2µm is proposed. In Article III the details of the fabrication method are expressed.

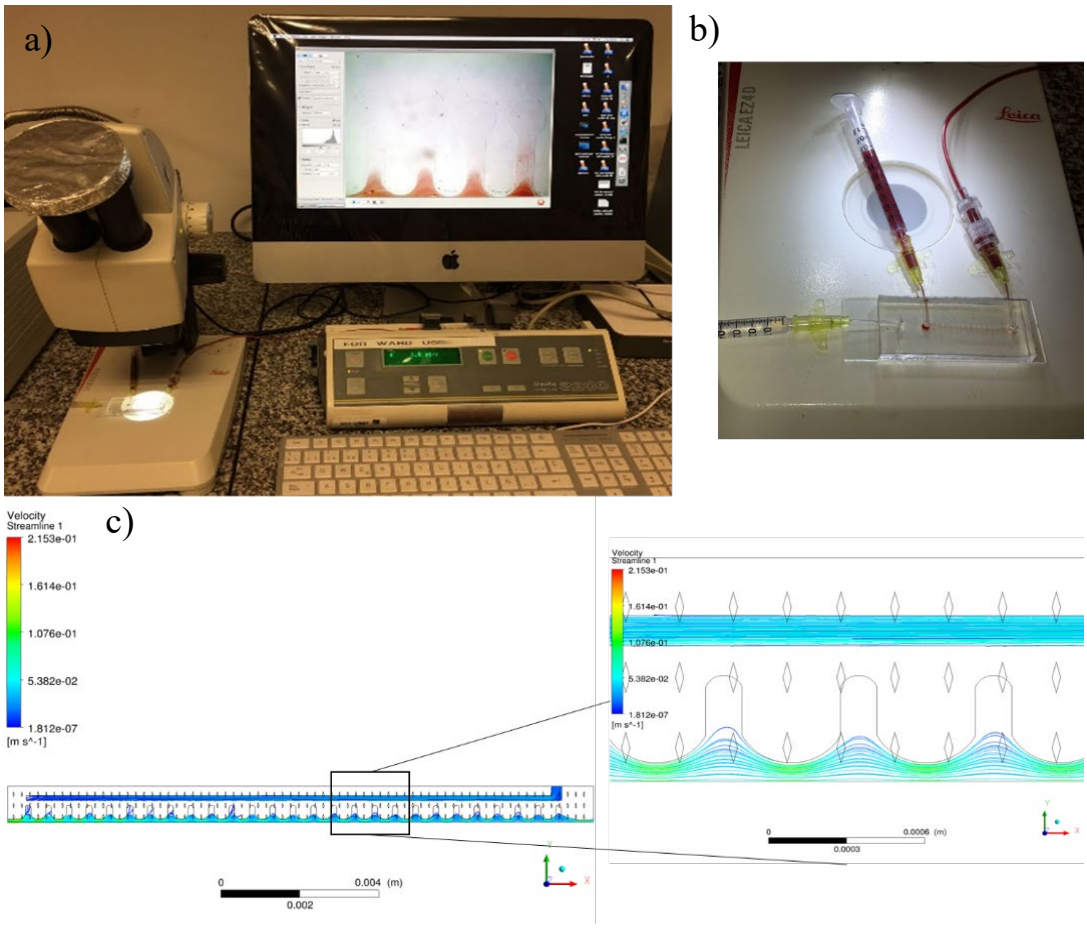

Figure 7. a) The experimental setup of the high-throughput BPS, b) The real BPS device, c) The 3-D simulated design of the corrugated channel.

Applications

Blood typing test

The blood typing test is obligatory in any pregnancy, transfusion, and organ transplant. Transfusion of non-compatible blood groups results in severe health problems that can be a serious, potentially fatal. Currently, more than thirty genetic-based blood typing methods are known [92]. Although, the ABO system [93] and the Rh system [94] are the most important ones in transfusion. This method was discovered by Karl Landsteiner in 1901. First, he patterned four major groups; A, B, AB, and O. The ABO blood group system denotes the presence of either A or B antigens on their RBC which indicate blood group A or B respectively, or a combination of A and B that is blood group AB or neither which is group O. The presence of antigen A on RBC means the absence of corresponding IgM antibodies in the serum. For instance, blood group A, always have antigen A on their RBCs and antibodies B in their serum. Rhesus (Rh) factor is an inherited protein found on the RBCs. If the blood has this protein, the group is Rh-positive, and the lack of this protein indicates the blood group as an Rh-negative. The mismatch of antigen and antibodies combination results in agglutination. Agglutinated blood cells can be detected from several sensitive and reliable assays such as the tube test, traditional slide test, the gel column agglutination, the microplate method, and the affinity column technology. These assays need special laboratory tools operated by trained laboratory staff, which increases the relative costs [95] and manipulation errors. Some of the modern technologies in ABO/Rh blood typing are synthetic/natural receptors, paper-based, molecular blood typing [96-99], emerging strategies, and blood test kits [95]. However, the conventional methods of blood typing are still considered the most reliable tests which are the most adopted in clinical laboratories [100]. In an emergency diagnosis situation, the lateral flow assays based on a functionalized cellulose membrane are more common but less accurate. Recently the Micronics ABO/Rh-Card provided a rapid, credit card-sized test for the simultaneous determination of an individual's ABO/Rh blood type from a finger prick sample of whole blood in 2 minutes [101]. A recent study of 26 fatal accidents due to the incompatibility of ABO/Rh showed that in 24% of the cases pre-transfusion bedside compatibility test (PBCT) was

not done at the patient bedside, in 32% the PBCT was not done at all, and in 44% it was done on the transfused unit and not to the patient. Human mistakes related to blood typing are cited as the most frequent cause of problems in transfusion. Another study of two commercial POCT showed that the error occurred in 30% of the assays. The errors were attributed to the poor technique of the operator, device failure or incorrect interpretation [102]. In order to decrease these errors, operating another method on the same sample to validate and enhance the accuracy of the primary results is needed. The direct (forward) method is based on a possible reaction of the antigens around the patients' RBCs with known antibodies while the indirect (reverse) method utilizes the reaction of natural antibodies from their plasma with identified RBCs. The comparison of the results from performing these two methods near the patient would significantly decrease the possible errors in blood typing. In other words, the indirect method is used to confirm results obtained in the direct method and in some countries, it is mandatory to perform both tests prior to a transfusion. To perform the indirect method the plasma needs to be extracted from blood. To this end, in order to have a POC blood grouping device, a BPS needs to divide a blood sample into five branches; three RBC outlets to test the direct method, and two plasma outlets for the indirect method. The combination of the microfluidic BPS, and the appropriate biomarkers to generate agglutination and visually detect the blood group leads to a stand-alone microchip which is capable of determining the blood grouping from both direct and indirect methods simultaneously (Figure 8) from a single droplet of blood.

The method of ABO/Rh blood typing in this device is based on the detection of agglutination on antigens of RBCs (direct method) and antibodies of plasma (indirect method). The differences between agglutinated and non-agglutinated samples are distinguishable by the naked eye as it is

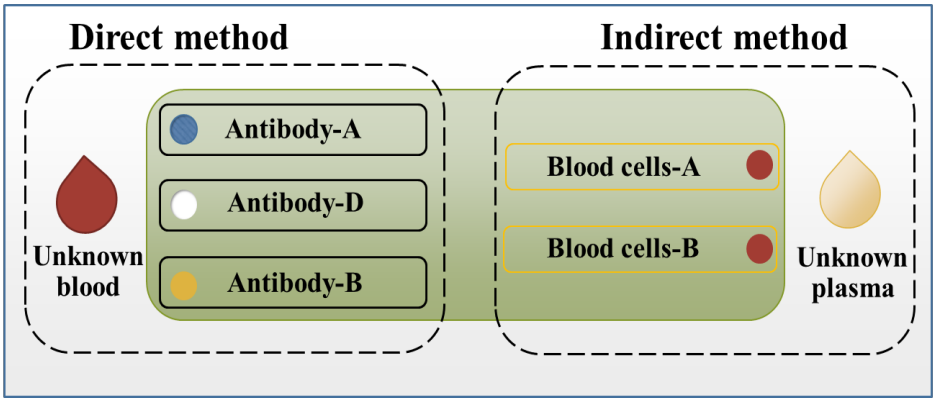

Figure 8. The schematic view of the proposed idea of the combination of both direct and indirect methods on a single cartridge.

shown in Figure 9 but also validated with particle analysis on the microscopic pictures. The results in this figure indicate the blood group A-positive since the mixture of antibody-A and antibody-D with the blood sample is positive. The positive reaction between RBC-B and the extracted plasma confirms this result. Additionally, the results of the passive BPS in ABO/Rh blood typing verified the quality and quantity of the extracted plasma in practical applications. This concept achieves fast, efficient, accurate, low cost and simple measurement of agglutination inside a passive microchip for both direct and indirect blood typing simultaneously.

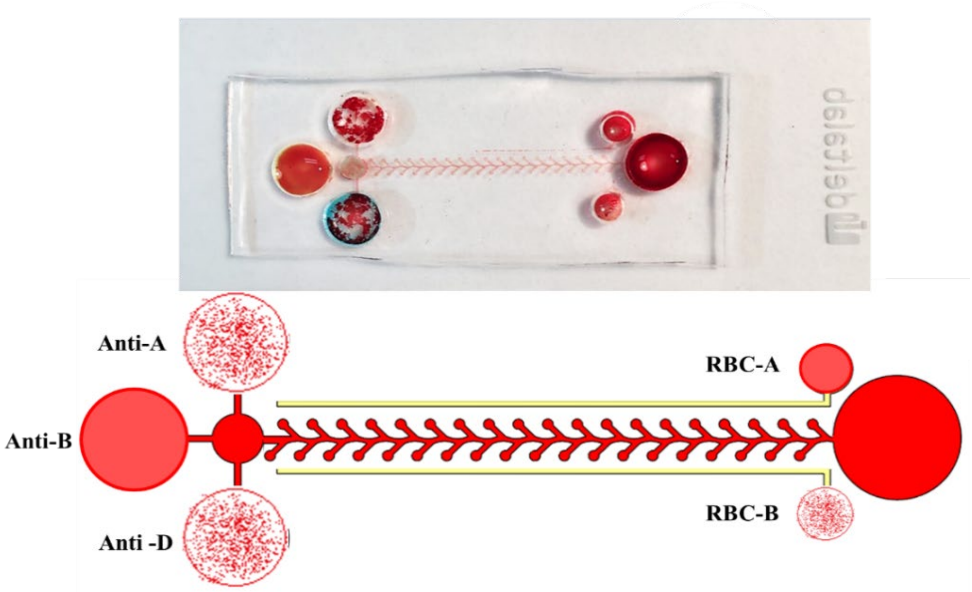

Figure 9. The schematic picture of the expected device and the real device. The reactions between antibodies and antigens results in agglutinations are visible by the naked eye.

Hemostasis level test

Hemostasis is a process to prevent bleeding in case of vascular injury, in fact, it happens when blood is presented outside of the body or blood vessels. It is the initial stage of wound healing and stops the body from loss of blood. This involves coagulation, blood changing from a liquid to a gel. During hemostasis three steps occur in a rapid sequence [103]. Vascular spasm is the first response as the blood vessels constrict to allow less blood to be lost. In the second step, platelet plug formation, platelets stick together to form a temporary seal to cover the break in the vessel

wall. The last step is called coagulation or blood clotting. Coagulation reinforces the platelet plug with fibrin threads that act as a molecular glue. Platelets are a large factor in the hemostatic process. They allow for the creation of the platelet plug that forms almost directly after a blood vessel has been ruptured. Within seconds of a blood vessel's epithelial wall being disrupted platelets begin to adhere to the sub-endothelium surface. It takes approximately sixty seconds until the first fibrin strands begin to intersperse among the wound. After several minutes the platelet plug is completely formed by fibrin. But if this process is deregulated or in other words thrombosis, it can because of cardiovascular diseases and can be life-threatening [104]. Thrombosis is the formation of a blood clot, known as a thrombus, within a blood vessel. It prevents blood from flowing normally through the circulatory system. The impact of thrombosis is increased by aging and an unhealthy lifestyle, therefore, providing a platform that leads to a better understanding of the hemostasis mechanism is needed. In order to evaluate the hemostasis process, the interaction of fibrin and platelets in blood clotting should be assessed which requires a combination of routine and specialized tests. Evaluation of hemorrhage (the opposite of hemostasis) also requires sophisticated equipment to identify the altered functional pathway and it is a time-consuming test. Analyzing the existence and function of the activators and inhibitors involving in the coagulation mechanism implies the thrombosis disorders diagnosis [105].

To improve the knowledge of the hemostasis process, microfluidics can help to mimic the blood vessels and ex vivo coagulation [106-108]. Currently, the limit of hemostasis evaluation is carrying out under static conditions, for instance on the plasma sample or enriched platelets suspensions [109]. These tests provide a fragmented view of the hemostasis, neglecting the interactions inside the blood vessels. Studies employing parallel chamber technologies and perfusion annular with circulating blood flow have provided remarkably to the knowledge on the function of the platelets in the thrombotic complications under shear conditions and the hemostatic mechanism [110,111]. Lately, the developed microfluidic systems have facilitated the implementation of perfusion assays compare to the classic approaches by using a smaller volume of blood samples and simplifying the evaluation of the results [106-108, 112]. Therefore, the study of blood flow biorheology is of great interest for a better understanding of hemostasis and the effects of antithrombotic drugs [97, 113]. Nowadays, microfluidic technologies and micro biomimetic flow chambers can provide a platform to study the concept of flow in blood coagulation and fibrin formation for the ex vivo situations [114-116]. Due to the employing of the direct oral anticoagulants (DOACs) to

circumvent the frequent monitoring and the dose adjustment with the classic Vitamin K antagonists (VKAs), there is a need to measure the effect of anticoagulant of the drugs in several situations such as bleeding or hospitalized or critically ill patients. Doubtfulness about the consumption of DOACs in patients requires an urgent invasive manner, uncertainty of overdose and recurrence of thrombotic events or the confirmation of adherence needs to be addressed [117,118]. Evaluation of the anticoagulant therapies is simple for VKAs, while it is very complex for the DOACs. Monitoring antiplatelet therapy or assessing the potential risk of bleeding or thrombosis requires specialized equipment and a definition of cutoff values for each drug. Unfortunately, the tests to determine the effects of DOACs on coagulation are drug-specific and are not regularly available in clinical laboratories. Within the help of the POC devices, the evaluation of the anticoagulant, the identification of a specific group of patients and the guidance of the reversal agents in case of overdose could be facilitated. Additionally, for the patients who are at the risk of cardiovascular complications, antiplatelet agents are prescribed, while monitoring their responses to these drugs is not demonstrated [119]. There are subgroups of patients in whom different laboratory tests indicate suboptimal responses to antiplatelet drugs. This condition, primarily, describes as resistance to the antiplatelet agent, has evolved to a more detailed concept of the patients with high on-treatment platelet reactivity (HPR) [120]. HPR exposes patients to an enhance of major adverse cardiovascular events risk and might require dual therapy. Conversely, the concept of low on-treatment platelet reactivity (LPR) defines subgroups of patients exposed to an increased risk of bleeding. The balance of efficacy vs. safety in subgroups of patients will be improved by the optimization of antiplatelet therapy based on a reliable functional assay. To develop a POC device that could evaluate the contribution of the platelets and coagulation elements of hemostasis in minutes of blood samples at patients' bedsides, the combination of both techniques is desired. In Article II, a fundamental contribution to a better understanding of the hemostasis process inside the vessels is presented to enhance the treatment of cardiovascular diseases. As a first step, designing a tool to characterize the behavior of plasma poor in platelets (PPP) and plasma rich in platelets (PRP) is required to create a reliable POC device for monitoring the antithrombotic treatment. During the last few years, DOACs were proposed to circumvent the frequent monitoring

of classical ones and decreased the burden on public health systems in countries where the growth of the elderly population has enhanced cardiovascular disease impact. But there is a need to measure the effectiveness of these treatments, especially at the patient's bedside. The use of biomimetic microfluidic channels for studying the hemostasis process reduces the time and the volume of required samples and provides a platform to analyze the results at the patient's bedside. In Article II, a novel microflow chamber as it is shown in Figure 10b, integrated to a replaceable biomimetic surface (Figure 10c) for evaluation of the hemostasis level is proposed. These two parts were assembled with the help of the 3D printed cascade which is illustrated in Figure 10a. This device requires a small amount of blood sample and reagents to perform the test in a reasonable time. The experimental set up of this system is shown in Figure 10d. A study about the APIX is done and compared with the previous conventional methods in order to validate the performance of this device. The results showed an excellent agreement while the volume of required samples was reduced. An interdigitated printed electrode is embedded in the chamber to measure the impedance during the coagulation procedure. This study could characterize the behavior of the PPP from PRP according to impedance measurement for the very first time.

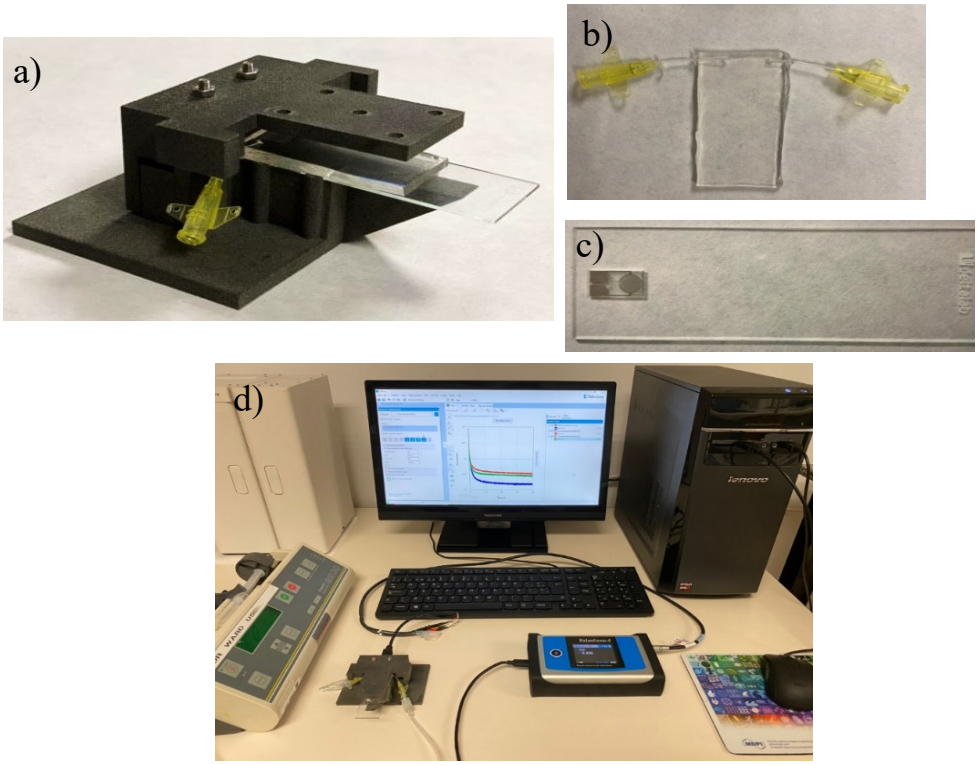

Figure 10. a) The 3D printed device assemble with the microflow chamber and biomimetic surface, b) The microflow chamber that is engraved on the PDMS and two connectors for inlet and outlet, c) The microelectrode integrated on the glass substrate, and d)The experimental setup of the measuring the hemostasis level of the PPP and PRP.

Fabrication

Nowadays with the advancement in microfluidics technology, a reliable, fast and cost-effective fabrication method is required to be able to compete with the conventional methods. Specifically, due to the complexity of the manufacturing process at the sub-micron range, most of them require a lithographic step which is time-consuming. Two of the main challenges facing low aspect ratio channels are proper bonding and avoidance of stiction. PDMS which is one of the most used materials in microfluidic systems due to its transparency, flexibility, and compatibility with biological applications, has a drawback of simply getting collapsed. PDMS can be processed with the soft-lithography method. This method is cost-effective and accurate but time-consuming. The schematic of the soft-lithography process to make a mold is illustrated in Figure 11. A glass substrate is the other candidate for biocompatible applications but the hose connections cannot be integrated easily. Besides, the wet-etching process that is schematically depicted in Figure 12 on the glass is time-consuming and has a huge environmental impact due to the extremely aggressive chemicals that are used to carve the channel. Therefore, it is difficult to be industrialized. Rapid prototyping in microfluidics enables prompt verifications in the experimental stage and avoids the

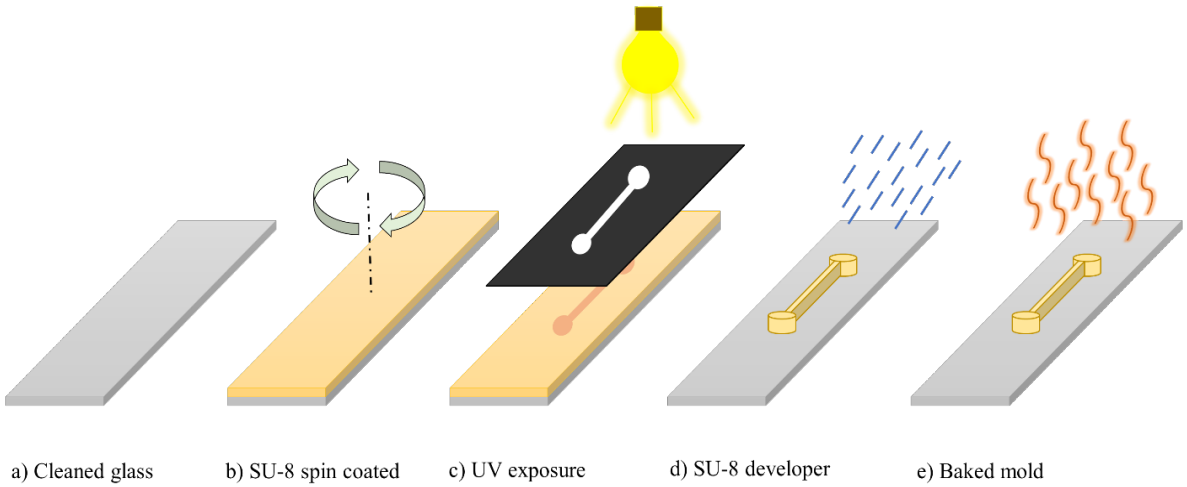

Figure 11. a) A clean and dry glass is used as a substrate, b) SU-8 is spun on to the glass to achieve the desired thickness, c) The sketch on the SU-8 is polymerized under the UV exposure, d) The polymerized glass is washed with SU-8 developer, and e) The created mold is baked.

need for simulations that are not 100% accurate. Therefore, there is a need for rapid and cost-effective manufacturing method especially in the sub-micron range that must be extremely reliable.

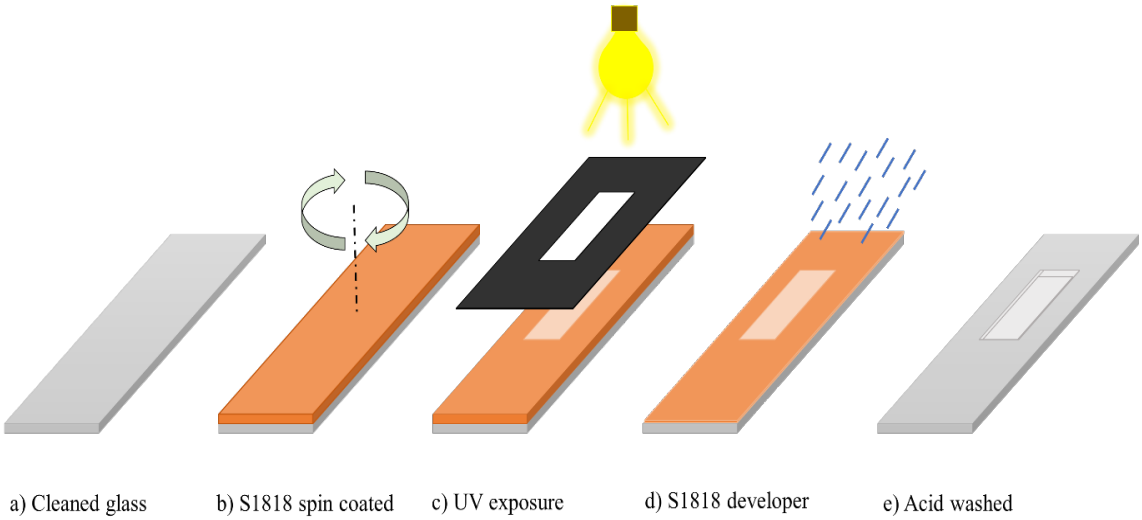

Figure 12. a) A clean and dry glass is used as a substrate, b) S1818 is spun on to the glass to achieve the desired thickness, c) The sketch on the S1818 is polymerized under the UV exposure, d) The exposed glass is washed by S1818 developer, and e) The glass is soaked in acid to achieve the desired depth inside the glass.

Article III introduced a direct laser microfabrication method that is capable of manufacturing sub-micron channels with a very low aspect ratio. This method uses an ultrashort pulse laser. In order to study the precision of this method, two parallel rectangles as shown in Figure 13 with different depth range (0.5 µm to 2 µm) and different width range (15 to 30 µm) are manufactured. Interferometric microscopy (S lynx Compact 3D Surface Profiler, SENSOFAR company in Spain) is used to measure the roughness of each pattern. Additionally, to evaluate the influence of the ultrashort pulse laser on the wettability of the glass, the static contact angle at each depth was measured (OCA 15EC, DataPhysics Instruments, Germany). Finally, the applicability of the manufactured sub-micron channel is validated by using it as a BPS device.

For a femtosecond laser, the laser-material interaction time is very short. Thus, heat energy has no time to diffuse in a lattice. The irradiated zone of the material quickly reaches the vaporization temperature and the ablated particles evaporate from the surface [121]. The results showed that the width of the channel does not have an influence on the surface roughness, while a higher depth, increased the roughness. The surface roughness for the depth of 0.5 µm was not uniform and some peaks appeared as it is shown in Figure 13. This is due to the number of laser passes. The first laser pass scratched the surface and the second laser pass unified the surface, this is why for all the depth

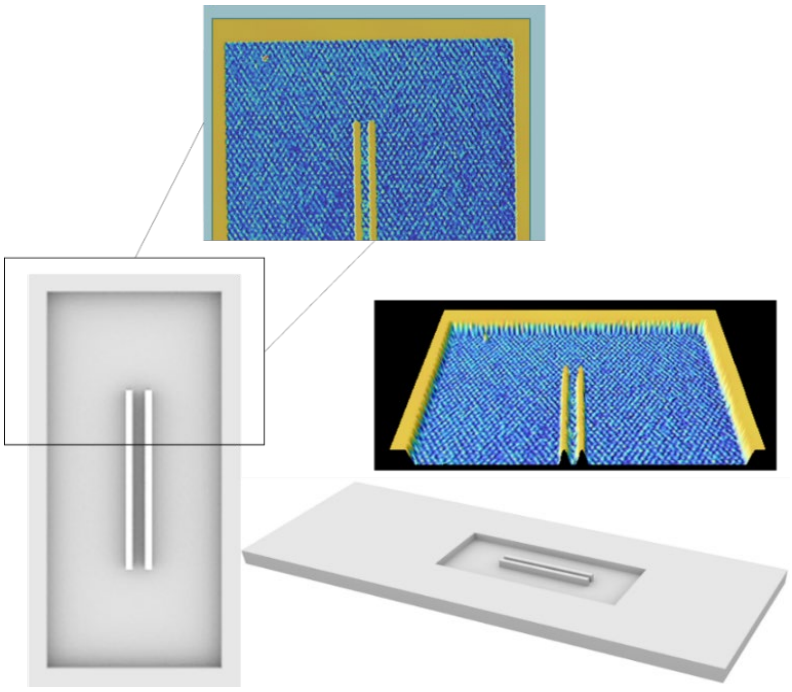

Figure 13. The schematic picture of the engraved glass by femtosecond laser and the microscopic view of the real glass.

that laser pass is an odd number (the case of 1-µm, 1.5-µm, and 2-µm-depth template) the roughness presents a maximum and at even number (the case of 0.75-µm, 1.25-µm, 1.75-µm depth template) the roughness improves. Additionally, the results showed increasing the depth, decreased the standard deviation. The measurement of the static contact angles on the patterns, irritated at laser passes of 2, 3, 4, 5, 6, and 7, denoted a dependency of the surface wettability on the laser passes, higher laser passes decreased the surface wettability but it revealed the hydrophilic behavior for all laser passes, which made it suitable for performing a self-driven test.

The open-top sub-micron channel with an array of pillars was manufactured using this process and the watertight property was reached by a PDMS cover to create the BPS. The plasma extracted with 100% purity and during the bonding process and operating the device there was no problem of collapsing due to the texture on the surface of the glass, which avoided stiction. This method had other advantages compared to current sub-micron watertight manufacturing methods. It was a faster manufacturing method for channel dimensions greater than 750 nm in-depth (about 40 seconds for a rectangle with the area of 18.5*12.5 mm2).

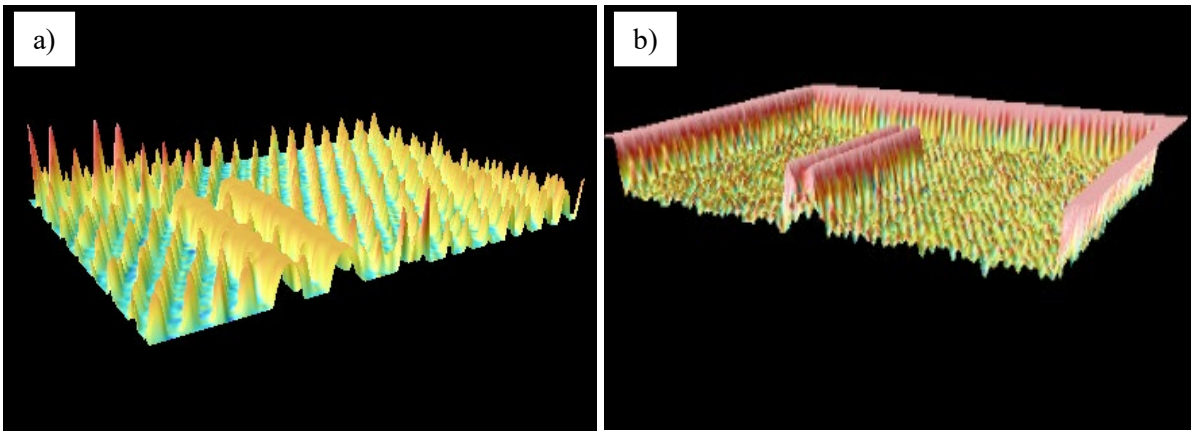

Figure 14. a) The microscopic picture of the surface with 0.5µm depth, patterned with one laser pass, b) the microscopic picture of the surface with 0.75µm depth patterned with two laser passes.

Conclusion

This thesis presents a series of improvements on a cross-flow filtration design for blood plasma separation. The main design has been modified to operate properly in both capillary and imposed flow conditions. In both cases, the appropriate performance has been accredited in practical applications: ABO/Rh blood typing and Hemostasis-on-Chip.

The hypothesis of enhancing the yield by keeping the 100% purity of the extracted plasma is validated by inducing the formation of air bubbles in the dead-end zones of the channels. A novel microfluidic channel with dead-end branches at each side was designed numerically using CFD modeling. The lopsided design with expansion-contraction geometry achieved a better RBC trapping in the branches. The presence of the dead-end zone at the end of each branch confined an air bubble that was disappearing during the process of separation. This modification not only increased the perimeter of the main channel to extract more plasma but also elongated the separation time by delaying the clogging process caused by the accumulation of RBCs in the main channel. The proposed design requires only a single droplet (50µl) of the whole blood without the need for any external forces or pre-analytical steps and a volume of 6-µl of plasma could be extracted in about 10 minutes with the highest purity level (100%). The microfluidic device was closed except for the inlet and outlet ports, protecting the reaction from environmental interference. The volume of the extracted plasma and its impressive purity can be successfully used for various diagnostic applications.

The proposed passive portable BPS is designed to perform the ABO/Rh blood typing from both direct and indirect methods. This chip operates with only blood a droplet while decreasing the processing time and manipulation errors. The detection of the blood typing is based on the agglutination which is visible by naked eyes and validated by microscopic pictures. Different blood types at different hematocrit ratios were analyzed using the proposed device. For hematocrit levels lower than 50% the results showed a good agreement in all four types of blood. This chip is more accurate than the chips in the market since it works with both direct and indirect methods

and the results from the indirect method are for validating the results from the direct method. This fact decreases manipulation errors.

Several modifications in the separation tank and the main channel were investigated to enhance the yield and purity for the high-throughput purpose. A 3-D CFD numerical simulation was performed to characterize the optimal design which provides a better separation at different flow rates. The numerical results are consistent with the experimental characterization of the device, which showed that the active BPS device has a better yield at a higher flow rate but lower purity. This is due to the flexibility of the PDMS that at the high shear rate it stretches and leads to the leakage of blood cells from the main channel. In contrast previous works, this has the potential to reach a yield as high as 19% with an acceptable purity of 77%. This BPS device not only worked with undiluted blood but also is reusable.

In Article II, a microchip has proposed that diagnoses the coagulation disorders with the help of impedance spectroscopy in a biomimetic approach. This device is microfabricated in the form of a microflow chamber with a replaceable biomimetic surface. The biomimetic surface embedded printed interdigitated gold electrodes to characterize the fibrinogen formation or platelets aggregation by reducing the requirement samples and testing time. The results showed a distinguishable behavior of PPP versus PRP. The change in PPP behavior was more noticeable at high frequencies while PRP showed a remarkable change at both low and high frequencies. This study is a base for the capability of POC devices for measuring the effect of anticoagulant on platelet aggregation or fibrinogen formation.

The previous findings are of direct practical application. The main current limitation is the existence of a batch fabrication method capable to produce the proposed geometries. In Article III, a novel rapid technique to manufacture a watertight sub-micron channel using femtosecond laser results in a successful definition of sub-micron channels from 500 nm and above. The width of the channel has higher accuracy for lower depth. For a channel with 1-µm-depth, the deviation in width was 0.4% while the accuracy regarding the depth increased with higher depth. This methodology has the potential to batch manufacture sub-micron channels essential in BPS devices. The technique was successfully used to extract plasma from blood with 100% purity. The findings suggest that this method has several advantages compared to current sub-micron watertight manufacturing methods. It takes about 40 seconds to create a rectangle with an area of 18.5*12.5

mm^2 while the mentioned conventional methods usually take several hours. Moreover, the intrinsic texture of the surface that is created while machining avoids collapse or obstruction of the small channels due to the deflection of the top layer. Based on the results, the number of laser passes has a significant influence on the aforementioned texture. The odd number of laser pass increased the surface roughness while the next laser pass decreased it. The number of laser passes had an impact on the contact angles: as the laser passes increased, the surface wettability decreased. Laser focus spot size limited the reduction of the width of the sub-micron channel. The glass maintained transparent which enables the colorimetric and particle counts analysis systems. From the outcome of this investigation, it is possible to conclude that the femtosecond laser is suitable for the batch fabrication of microfluidic BPS.

Future works

Current findings suggest that the approach of cross-flow filtration and hydrodynamic separation can be useful for plasma extraction and its application to different diagnostic purposes. Aside from the already shown applications in ABO/Rh blood grouping and hemostasis studies, the BPS has the potential to miniaturize enzyme-linked immunosorbent assay (μELISA) and other current diagnostic techniques. The addition of a mixer to the BPS would enhance could provide portability to ELISA in conventional diagnostic tool in medicine but also in plant pathology, and biotechnology, as well as a quality control check in various industries. Many of the applications requires the extracted plasma or fluid to be mixed with specific regents. Therefore, designing a mixer compatible with the separation times and the volumes provides is required.

The results from the proposed device suggest that this approach could also be useful for isolation of other cells by their size. For instance, the circulating tumor cells (CTC) from cerebrospinal fluid (CSF), Mycobacterium tuberculosis bacteria (MTB) from saliva or and parasites from blood.

CTCs in CSF are very rare but if present it is a clear sign for the diagnosis of certain illnesses. CSF volume in adults ranges from 125 mL to 150mL [112] and its collection process is not very pleasant. Therefore, finding a way to decrease the sample requirement for CTC detection is desired. For this matter, the same strategy of our BPS design to sort cancer tumor cells is suggested. The CSF can pass through the channel and only CTCs which are bigger in size will be trapped in the main channel. Besides, the septation of CTCs from whole blood which are also very rare in numbers compared to millions of blood cells in blood, is a challenge due to the need to process in continuous an important volume of sample to only detect few cells. But this capability could provide for the first time a CTC detection device for POC testing. One idea is to lyse the RBCs and sort the WBCs and CTCs by their size to isolate the CTCs.

The other application is tuberculosis detection, which the biggest challenge is in the prompt diagnosis of TB. By redesigning the BPS device for capturing the MTB from saliva, a platform for detecting and trapping these bacteria could be prepared. This method should be sensitive, rapid, and is expected to find use in resource-limited settings where TB is still the one of the most prevalent illness.

Parasites can be present in very low numbers, sometimes lower than 1 per µl blood compared to the millions of red blood cells in the same volume [122]. The problems are the same for other types of rare cells. In addition, clinical analysis of acute viral infection in blood requires the separation of viral particles from blood cells, since the aforementioned microfluidic device can use to continuously purify blood from viral particles like HIV particles.

Doubtlessly in the near future, significant advances in POCT due to the emerging technologies, will reduce the health-care costs and lead to improve diagnostics systems. These advances will empower patients and the general population by providing them with personalized devices equipped with tools for preventive medicine, mobile health care, and telemedicine [123].

References

1. *Microfluidics Market by Application (Genomics, Proteomics, Capillary Electrophoresis, IVD (POC, Clinical Diagnostics), Drug Delivery, Microreactor, Lab Tests), Component (Chips, Pump, Needle), Material (Polymer, Glass, Silicon) - Global Forecast to 2023.*
2. *Yang S, Ündar A, Zahn JD. A microfluidic device for continuous, real time blood plasma separation. Lab on a Chip. 2006;6(7):871-80.*
3. *Shatova TA, Lathwal S, Engle MR, Sikes HD, Jensen KF. Portable, constriction–expansion blood plasma separation and polymerization-based malaria detection. Analytical chemistry. 2016 Jul 13;88(15):7627-32.*
4. *Kim B, Oh S, You D, Choi S. Microfluidic pipette tip for high-purity and high-throughput blood plasma separation from whole blood. Analytical chemistry. 2017 Jan 11;89(3):1439-44.*
5. *Prabhakar A, Kumar YB, Tripathi S, Agrawal A. A novel, compact and efficient microchannel arrangement with multiple hydrodynamic effects for blood plasma separation. Microfluidics and Nanofluidics. 2015 May 1;18(5-6):995-1006.*
6. *Kersaudy-Kerhoas M, Kavanagh DM, Dhariwal RS, Campbell CJ, Desmulliez MP. Validation of a blood plasma separation system by biomarker detection. Lab on a Chip. 2010;10(12):1587-95.*
7. *S. Tripathi, Y. V. B. Kumar, A. Agrawal, and A. Prabhakar, "Microdevice for plasma separation from whole human blood using bio- physical and geometrical effects," Nat. Publ. Gr., no. April, pp. 1–15, 2016.*
8. *Austin AW, Wissmann T, von Kanel R. Stress and hemostasis: an update. InSeminars in thrombosis and hemostasis 2013 Nov (Vol. 39, No. 08, pp. 902-912). Thieme Medical Publishers.*
9. *Favaloro EJ, Franchini M, Lippi G. Aging hemostasis: changes to laboratory markers of hemostasis as we age—a narrative review. InSeminars in thrombosis and hemostasis 2014 Sep (Vol. 40, No. 06, pp. 621-633). Thieme Medical Publishers.*
10. *https://www.fluigent.com/microfluidic-expertise/what-is-microfluidic/microfluidic-definitions-and-advantages/*
11. *Maciel GD, Santos HK, Ferreira FD. Rheological analysis of water clay compositions in order to investigate mudflows developing in canals. Journal of the Brazilian Society of Mechanical Sciences and Engineering. 2009 Mar;31(1):64-74.*
12. *Blue CM. Darby's Comprehensive Review of Dental Hygiene-E-Book. Elsevier Health Sciences; 2015 Dec 21.*

13. *Chee CY, Lee HP, Lu C. Using 3D fluid–structure interaction model to analyse the biomechanical properties of erythrocyte. Physics Letters A. 2008 Feb 25;372(9):1357-62*
14. *Geyer PE, Holdt LM, Teupser D, Mann M. Revisiting biomarker discovery by plasma proteomics. Molecular systems biology. 2017 Sep 1;13(9).*
15. *Acker JP, Marks DC, Sheffield WP. Quality assessment of established and emerging blood components for transfusion. Journal of blood transfusion. 2016;2016.*
16. *Karimi S, Mehrdel P, Farré-Lladós J, Casals-Terré J. A passive portable microfluidic blood–plasma separator for simultaneous determination of direct and indirect ABO/Rh blood typing. Lab on a Chip. 2019;19(19):3249-60.*
17. *Yager P, Edwards T, Fu E, Helton K, Nelson K, Tam MR, Weigl BH. Microfluidic diagnostic technologies for global public health. Nature. 2006 Jul;442(7101):412.*
18. *Demello AJ. Control and detection of chemical reactions in microfluidic systems. Nature. 2006 Jul;442(7101):394.*
19. *Santrach PJ. Current & future applications of point of care testing. Mayo Clinic, www. cdc. gov Search PubMed. 2012.*
20. *Mielczarek WS, Obaje EA, Bachmann TT, Kersaudy-Kerhoas M. Microfluidic blood plasma separation for medical diagnostics: is it worth it?. Lab on a Chip. 2016;16(18):3441-8.*
21. *Kersaudy-Kerhoas M, Sollier E. Micro-scale blood plasma separation: from acoustophoresis to egg-beaters. Lab on a Chip. 2013;13(17):3323-46.*
22. *R. Gorkin, J. Park, J. Siegrist, M. Amasia, B. S. Lee, J. M. Park, J. Kim, H. Kim, M. Madou and Y. K. Cho, Lab Chip, 2010, 10, 1758–1773.*
23. *J. Steigert, M. Grumann, T. Brenner, K.Mittenbu¨hler, T. Nann, J. Ru¨he, I. Moser, S. Haeberle, L. Riegger, J. Riegler,W. Bessler, R. Zengerle and J. Ducre´e, J. Assoc. Lab. Autom., 2005, 10, 331–341.*
24. *M. Amasia and M. Madou, Bioanalysis, 2010, 2, 1701–1710.*
25. *C. T. Schembri, V. Ostoich, P. J. Lingane, T. L. Burd and S. N. Buhl, Clin. Chem., 1992, 38, 1665–1670.*
26. *S. Haeberle, T. Brenner, R. Zengerle and J. Ducree, Lab Chip, 2006, 6, 776–781.*
27. *Tripathi S, Kumar YB, Agrawal A, Prabhakar A, Joshi SS. Microdevice for plasma separation from whole human blood using bio-physical and geometrical effects. Scientific reports. 2016 Jun 9;6:26749.*

28. *Jeong, G. S., Chung, S., Kim, C. B. & Lee, S. H. Applications of micromixing technology. Analyst. 135, 460–473 (2010).*
29. *E. Carrilho, A. W. Martinez and G. M. Whitesides, Anal. Chem., 2009, 81, 7091–7095.*
30. *X. Li, D. R. Ballerini and W. Shen, Biomicrofluidics, 2012, 6, 011301.*
31. *Alere, Alere Cholestech LDX® System, http://www.alere.com/us/en/product-details/cholestech-ldx-system.html,2013.*
32. *CoaguChek, CoaguChek® systems are easy to use, http://www.coaguchek.com/uk/index.php?target=/en/patients/products.*
33. *X. Yang, O. Forouzan, T. P. Brown and S. S. Shevkoplyas, Lab Chip, 2012, 12, 274–280.*
34. *T. Songjaroen, W. Dungchai, O. Chailapakul, C. S. Henry and W. Laiwattanapaisal, Lab Chip, 2012, 12, 3392–3398.*
35. *M. L. Brigden, American Family Physician, 1999, 60, 1443–1450.*
36. *S. Y. Yoon, S. Yang, Y. Moon and K. C. Kim, presented in part at MicroTas 2006, Tokyo, Japan, 2006.*
37. *T. Tachi, N. Kaji, M. Tokeshi and Y. Baba, Anal. Chem., 2009, 81, 3194–3198.*
38. *C. T. Huang, H. H. Chang, P. N. Li and C. P. Jen, presented in part at the 5th IEEE International Conference on Nano/Micro Engineered and Molecular Systems, Xiamen, China, 2010.*
39. *C.T. Huang, P. N. Li, C. Y. Pai, T. S. Leu and C. P. Jen, Sep. Sci. Technol., 2010, 45, 42–49.*
40. *I. K. Dimov, L. Basabe-Desmonts, J. L. Garcia-Cordero, B. M.Ross,A. J.Ricco and L. P. Lee, Lab Chip, 2011, 11, 845–850.*
41. *Michael G. M., Changchun L., Jinzhao S. and Haim H. B., Integrated Microfluidic Nucleic Acid Isolation, Isothermal Amplification, and Amplicon Quantification, Microarrays 2015, 4, 474-489.*
42. *X. B. Zhang, Z. Q. Wu, K. Wang, J. Zhu, J. J. Xu, X. H. Xia and H. Y. Chen, Anal. Chem., 2012, 84, 3780–3786.*
43. *S. Thorslund, O. Klett, F. Nikolajeff, K. Markides and J. Bergquist, Biomed. Microdevices, 2006, 8, 73–79.*
44. *S. Wang, D. Sarenac, M. H. Chen, S. H. Huang, F. F. Giguel, D. R. Kuritzkes and U. Demirci, International Journal of Nanomedicine, 2012, 7, 5019–5028.*
45. *J. Moorthy and D. J. Beebe, Lab Chip, 2003, 3, 62–66.*
46. *C. Li, C. Liu, Z. Xu and J. Li, Biomed. Microdevices, 2012, 14, 565–572.*
47. *K. H. Chung, Y. H. Choi, J. H. Yang, C. W. Park, W. J. Kim, C. S. Ah and G. Y. Sung, Lab Chip, 2012, 12, 3272–3276.*

48. *C.B. Raub. Lee, E. Kartalov, Sequestration of bacteria from whole blood by optimized microfluidic cross-flow filtration for Rapid Antimicrobial Susceptibility Testing., Sensors and Actuators B 210 2015 120–123.*
49. *Z. Li, Y. Wang, J. Wang, Z. Tang, J.G. Pounds, Y. Lin, Rapid and sensitive detection of protein biomarker using a portable fluorescence biosensor based on quantum dots and a lateral flow test strip, Anal. Chem. 82 (2010) 7008–7014.*
50. *T. A. Crowley and V. Pizziconi, Lab Chip, 2005, 5, 922–929.*
51. *V. VanDelinder and A. Groisman, Anal. Chem., 2006, 78, 3765–3771.*
52. *E. Sollier, H. Rostaing, P. Pouteau, Y. Fouillet and J. L. Achard, Sens. Actuators, B, 2009, 141, 617–624.*
53. *K. Aran, A. Fok, L. A. Sasso, N. Kamdar, Y. Guan, Q. Sun, A. Undar and J. D. Zahn, Lab Chip, 2011, 11, 2858–2868.*
54. *T. M. Squires and S. R. Quake, Rev. Mod. Phys., 2005, 77, 977–1026.*
55. *G. B. Thurston, Biorheology, 1989, 26, 199–214.*
56. *D. Di Carlo, Lab Chip, 2009, 9, 3038–3046.*
57. *E. Sollier, in Microfluidic Technologies for Human Health, World Scientific Publishing Company, 2012.*
58. *S. C. Hur, H. T. K. Tse and D. Di Carlo, Lab Chip, 2010, 10, 274–280.*
59. *G. Segre´ and A. Silberberg, Nature, 1961, 189, 209–210.*
60. *P. M. van Midwoud, A. Janse, M. T. Merema, G. M. Groothuis and E. Verpoorte, Anal. Chem., 2012, 84, 3938–3944.*
61. *E. Sollier, H. Rostaing, P. Pouteau, Y. Fouillet and J. L. Achard, Sens. Actuators, B, 2009, 141, 617–624.*
62. *James P. L., Microfluidic tangential flow filter and continuous-flow reactor for bioprocess development, University College London, PhD thesis, 2015*
63. *B. S. Lee, J.N. Lee, J.M. Park, J.G. Lee, S. Kim, Y.K. Cho and C. Ko, Lab Chip, 2009, 9, 1548–1555.*
64. *S. Choi and J. K. Park, presented in part at the microTAS 2007, Paris, 2007.*
65. *S. Yang, A. Undar and J. D. Zahn, Lab Chip, 2006, 6, 871–880.*
66. *S. Yang, A. Undar and J. D. Zahn, ASAIO J., 2005, 51, 585–590.*
67. *E. Sollier, M. Cubizolles, Y. Fouillet and J.-L. Achard, Biomed. Microdevices, 2010, 12, 485–497.*

68. *M. Kersaudy-Kerhoas, R. Dhariwal, M. P. Y. Desmulliez and L. Jouvet, Microfluid. Nanofluid., 2010, 8, 105–114.*
69. *A. J. Mach and D. Di Carlo, Biotechnol. Bioeng., 2010, 107, 302–311.*
70. *A. Lenshof, A. Ahmad-Tajudin, K. Ja¨rås, A. M. Swa¨rd-Nilsson, L. Åberg, G. r. Marko-Varga, J. Malm, H. Lilja andT. Laurell, Anal. Chem., 2009, 81, 6030–6037.*
71. *F. Petersson, A. Nilsson, C. Holm, H. Jonsson andT. Laurell, Lab Chip, 2005, 5, 20–22.*
72. *F. Petersson, L. Aberg, A. M. Sward-Nilsson and T. Laurell, Anal. Chem., 2007, 79, 5117–5123.*
73. *T. Laurell, F. Petersson and A. Nilsson, Chem. Soc. Rev., 2007, 36, 492–506.*
74. *A. Lenshof and T. Laurell, Chem. Soc. Rev., 2010, 39, 1203–1217.*
75. *C. M. Das, F. Becker, S. Vernon, J. Noshari, C. Joyce and P. R. Gascoyne, Anal. Chem., 2005, 77, 2708–2719.*
76. *Mohammadi M, Madadi H, Casals-Terré J, Sellarès J. Hydrodynamic and direct-current insulator-based dielectrophoresis (H-DC-iDEP) microfluidic blood plasma separation. Analytical and bioanalytical chemistry. 2015 Jun 1;407(16):4733-44.*
77. *Mohammadi M, Madadi H, Casals-Terré J. Microfluidic point-of-care blood panel based on a novel technique: Reversible electroosmotic flow. Biomicrofluidics. 2015 Sep 11;9(5):054106.*
78. *S. A. Peyman, E. Y. Kwan, O. Margarson, A. Iles an N. Pamme, J. Chromatogr., A, 2009, 1216, 9055–9062.*
79. *A. I. Rodriguez-Villarreal, M. D. Tarn, L. A. Madden, J. B. Lutz, J. Greenman, J. Samitier and N. Pamme, Lab Chip, 2011, 11, 1240–1248.*
80. *N. Pamme and C. Wilhelm, Lab Chip, 2006, 6, 974–980.*
81. *K. H. Han and A. B. Frazier, Lab Chip, 2006, 6, 265–273.*
82. *J. Jung and K. H. Han, Appl. Phys. Lett., 2008, 93, 223902.*
83. *C. W. Yung, J. Fiering, A. J. Mueller and D. E. Ingber, LabChip, 2009, 9, 1171–1177.*
84. *Shields IV CW, Reyes CD, López GP. Microfluidic cell sorting: a review of the advances in the separation of cells from debulking to rare cell isolation. Lab on a Chip. 2015;15(5):1230-49.*
85. *Eluru G, Nagendra P, Gorthi SS. Microfluidic In-Flow Decantation Technique Using Stepped Pillar Arrays and Hydraulic Resistance Tuners. Micromachines. 2019 Jul;10(7):471.*
86. *Kim B, Oh S, You D, Choi S. Microfluidic pipette tip for high-purity and high-throughput blood plasma separation from whole blood. Analytical chemistry. 2017 Jan 11;89(3):1439-44.*
87. *Kersaudy-Kerhoas M, Kavanagh DM, Dhariwal RS, Campbell CJ, Desmulliez MP. Validation of a blood plasma separation system by biomarker detection. Lab on a Chip. 2010;10(12):1587-95.*
88. *Mitra SK, Chakraborty S. Microfluidics and Nanofluidics Handbook: Chemistry, physics, and life science principles. CRC Press; 2011 Sep 20.*

89. J. C. Erik, "The margination and transport of particles in blood flow," Doctoral Dissertations, 2017.
90. H. Madadi, J. Casals-Terré, M. Mohammadi. Self-driven filter-based blood plasma separator microfluidic chip for point-of-care testing. Biofabrication. 2015 May 22;7(2):025007.
91. Fahraeus R, Lindqvist T. The viscosity of the blood in narrow capillary tubes. American Journal of Physiology-Legacy Content. 1931 Mar 1;96(3):562-8.
92. Z. Liu, M. Liu, T. Mercado, O. Illoh, R. Davey. Extended blood group molecular typing and next-generation sequencing. Transfus. Med. Rev. 2014, 28, 177–186. [CrossRef] [PubMed]
93. K. Landsteiner. Zur Kenntnis der antifermentativen lytischen and agglutinierendenWirkung des Blutserums and der lymph. Zentralbl. Bakteriol. Parasit. Infekt. 1900, 27, 357–362.
94. K. Landsteiner. Ueber Agglutinationserscheinungen normalen menschlichen Blutes. Wien. Klin. Wochenschr. 1901, 14, 1132–1134.
95. W. Malomgré, B. Neumeister. Recent and future trends in blood group typing. Analytical and bioanalytical chemistry. 2009 Mar 1;393(5):1443-51.
96. M. Li, WL. Then, L. Li, W. Shen. Based device for rapid typing of secondary human blood groups. Analytical and bioanalytical chemistry. 2014 Jan 1;406(3):669-77.
97. J. Noiphung, K. Talalak, I. Hongwarittorrn, N. Pupinyo, P. Thirabowonkitphithan, W. Laiwattanapaisal. A novel paper-based assay for the simultaneous determination of Rh typing and forward and reverse ABO blood groups. Biosensors and Bioelectronics. 2015 May 15; 67:485-9.
98. WL. Then, M. Li, H. McLiesh, W. Shen, G. Garnier. The detection of blood group phenotypes using paper diagnostics. Vox sanguinis. 2015 Feb 1;108(2):186-96.
99. M. Al-Tamimi, W. Shen, R. Zeineddine, H. Tran, G. Garnier. Validation of paper-based assay for rapid blood typing. Analytical chemistry. 2012 Jan 9;84(3):1661-8.
100. M. Adnan, L.D. Franz. Blood Group Typing: From Classical Strategies to the Application of Synthetic Antibodies Generated by Molecular Imprinting. Sensors 2016, 16, 51; doi:10.3390/s16010051.
101. https://www.micronics.net/products/diagnostic-products/immunohematology
102. H. Maxime, C. Myriam, B. Arnaud. Red blood cell agglutination for blood typing within passive microfluidic biochips. High-throughput MDPI 2018, (10).
103. https://opentextbc.ca/anatomyandphysiology/chapter/18-5-hemostasis/
104. https://courses.lumenlearning.com/boundless-ap/chapter/hemostasis/

105. Paniccia R, Priora R, Liotta AA, Abbate R. Platelet function tests: a comparative review. Vascular health and risk management. 2015;11:133.

106. Neeves, K.B.; Onasoga, A.A.; Wufsus, A.R. The use of microfluidics in hemostasis: Clinical diagnostics and biomimetic models of vascular injury. Curr. Opin. Hematol. 2013, 20, 417–423.

107. Shen, F.; Kastrup, C.J.; Liu, Y.; Ismagilov, R.F. Threshold Response of Initiation of Blood Coagulation by Tissue Factor in Patterned Microfluidic Capillaries Is Controlled by Shear Rate. Arterioscler. Thromb. Vasc. Biol. 2008, 28, 2035–2041.

108. Li, M.; Ku, D.N.; Forest, C.R. Microfluidic system for simultaneous optical measurement of platelet aggregation at multiple shear rates in whole blood. Lab Chip 2012, 12, 1355.

109. Michelson, A.D. Methods for the measurement of platelet function. Am. J. Cardiol. 2009, 103, 20A–26A.

110. Sakariassen, K.S.; Houdijk, W.P.; Sixma, J.J.; Aarts, P.A.; de Groot, P.G. A perfusion chamber developed to investigate platelet interaction in flowing blood with human vessel wall cells, their extracellular matrix, and purified components. J. Lab Clin. Med. 1983, 102, 522–535.

111. Escolar, G.; Mazzara, R.; Castillo, R.; Ordinas, A. The role of the Baumgartner technique in transfusion medicine: Research and clinical applications. Transfusion 1994, 34, 542–549.

112. Nagy, M.; Heemskerk, J.W.; Swieringa, F. Use of microfluidics to assess the platelet-based control of coagulation. Platelets 2017, 28, 441–448.

113. Fedosov, D.A.; Dao, M.; Karniadakis, G.E.; Suresh, S. Computational Biorheology of Human Blood Flow in Health and Disease. Ann. Biomed. Eng. 2014, 42, 368–387.

114. Jain, A.; van der Meer, A.D.; Papa, A.L.; Barrile, R.; Lai, A.; Schlechter, B.L.; Otieno, M.A.; Louden, C.S.; Hamilton, G.A.; Frelinger, A.L.; et al. Assessment of whole blood thrombosis in a microfluidic device lined by fixed human endothelium. Biomed. Microdevices 2016, 18, 73.

115. Zhang, Y.S.; Davoudi, F.; Walch, P.; Manbachi, A.; Luo, X.; Dell'Erba, V.; Miri, A.K.; Albadawi, H.; Arneri, A.; Wang, X.; et al. Bioprinted thrombosis-on-a-chip. Lab Chip 2016, 16, 4097–4105.

116. Jain, A.; Graveline, A.; Waterhouse, A.; Vernet, A.; Flaumenhaft, R.; Ingber, D.E. A shear gradient-activated microfluidic device for automated monitoring of whole blood haemostasis and platelet function. Nat. Commun. 2016, 7, 10176.

117. Patel, M.R.; Hellkamp, A.S.; Fox, K.A. Point-of-Care Warfarin Monitoring in the ROCKET AF Trial. N. Engl. J. Med. 2016, 374, 785–788.

118. Hori, M.; Ohashi, Y.; Pan, G.; Kato, M.; Kajikawa, M. Point-of-Care Device for Warfarin Monitoring Used in the J-ROCKET AF Study. Circ. J. 2016, 80, 1488–1490.

119. Cattaneo, M. Resistance to antiplatelet drugs: Molecular mechanisms and laboratory detection. J. Thromb. Haemost. 2007, 5, 230–237.

120. Lenk, E.; Spannagl, M. Platelet Function Testing—Guided Antiplatelet Therapy EJIFCC 2014, 24, 90.

121. Zhang D, Guan L. Laser ablation.

122. Beech J. Microfluidics Separation and Analysis of Biological Particles. Fasta Tillståndets Fysik, 2011. 215 p.

123. Vashist SK, Luppa PB, Yeo LY, Ozcan A, Luong JH. Emerging technologies for next-generation point-of-care testing. Trends in biotechnology. 2015 Nov 1;33(11):692-705.

A passive portable microfluidic blood–plasma separator for simultaneous determination of direct and indirect ABO/Rh blood typing

Shadi Karimi, Pouya Mehrdel, Josep Farré-Lladós and Jasmina Casals-Terré *

The blood typing test is mandatory in any transfusion, organ transplant, and pregnancy situation. There is a lack of point-of-care (POC) blood typing that could perform both direct and indirect methods using a sin- gle droplet of whole blood. This study presents a new methodology combining a passive microfluidic blood–plasma separator (BPS) and a blood typing detector for the very first time, leading to a stand-alone microchip which is capable of determining the blood group from both direct and indirect methods simul- taneously. The proposed design separates blood cells from plasma by applying hydrodynamic forces im- posed on them, which overcomes the clogging issue and consequently maximizes the volume of the extracted plasma. An axial migration effect across the main channel is responsible for collecting the plasma in plasma collector channels. The BPS novel design approached 12% yield of plasma with 100% purity in approximately 10 minutes. The portable BPS was designed and fabricated to perform ABO/Rh blood tests based on the detection of agglutination in both antigens of RBCs (direct) and antibodies of plasma (indi- rect). The differences between agglutinated and non-agglutinated samples were distinguishable by the na- ked eye and also validated by particle analysis of microscopic pictures. The results of this passive BPS in ABO/Rh blood grouping verified the quality and quantity of the extracted plasma in practical applications

micromachines

MDPI

Article

Hemostasis-On-a-Chip: Impedance Spectroscopy Meets Microfluidics for Hemostasis Evaluation

Shadi Karimi [1], Josep Farré-Lladós [1], Enrique Mir [2,3], Ginés Escolar [3] and Jasmina Casals-Terré [1,*]

1 Mechanical Engineering Department–MicroTech Lab., Universitat Politècnica de Catalunya, Colom 7-11, 08222 Terrassa, Spain
2 Instituto de Investigación contra la Leucemia Josep Carreras, Muntaner 383, 08021 Barcelona, Spain
3 Servicio de Hemoterapia y Hemostasia, Hospital Clínic de Barcelona, Instituto de Investigaciones Biomédica August Pi i Sunyer (IDIBAPS), Universidad de Barcelona, 08007 Barcelona, Spain
* Correspondence: Jasmina.casals@upc.edu; Tel.: +34-937-398023

Received: 5 June 2019; Accepted: 12 August 2019; Published: 14 August 2019

Abstract: In the case of vascular injury, a complex process (of clotting) starts, involving mainly platelets and coagulation factors. This process in healthy humans is known as hemostasis, but when it is deregulated (thrombosis), it can be the cause of important cardiovascular diseases. Nowadays, the aging of the population and unhealthy lifestyles increase the impact of thrombosis, and therefore there is a need for tools to provide a better understanding of the hemostasis mechanisms, as well as more cost-effective diagnosis and control devices. This study proposes a novel microflow chamber, with interchangeable biomimetic surfaces to evaluate global hemostasis, using reduced amounts of blood sample and reagents, and also a minimized time required to do the test. To validate the performance of this novel device, a study on the new oral anticoagulant Apixaban (APIX) has been performed and compared to previous conventional techniques. The test shows an excellent agreement, while the amount of the required sample has been reduced (only 100 µL is used), and the amount of reagent as well. An imprinted electrode embedded in the chamber in order to measure the impedance during the coagulation process. This approach distinguishes the impedance behavior of plasma poor in platelets (PPP) and plasma rich in platelets (PRP) for the first time.

Keywords: organ-on-a-chip; vein-on-a-chip; impedance; microfluidics; hemostasis

1. Introduction

Hemostasis is the result of the collaboration between plasma and blood cells to stop bleeding during the initial steps of wound healing. Current unhealthy habits and aging of the population alter the physiologic balance of blood coagulation, resulting in thrombotic complications. During thrombosis, the aggregation of platelets and coagulation products can prevent blood flow and cause damage in downstream organs, resulting in ischemia and/or tissue death.

Evaluation of hemostasis requires a combination of routine and specialized tests to assess the interaction of platelet and fibrin components involved in blood clotting. Evaluation of hemorrhagic disorders does also require time-consuming tests and sophisticated equipment to identify the altered functional pathways. The diagnosis of thrombotic disorders implies the analysis of the presence and function of activators and inhibitors participating in these coagulation mechanisms.

Nowadays, the evaluation of hemostasis is performed under static conditions. The introduction of microfluidics approaches provides the possibility to mimic blood flow and ex vivo coagulation with minute volume samples, therefore it is already being used as an important tool to improve the knowledge on hemostasis processes [1–3].

A common limitation of the majority of current tests applied to the evaluation of hemostasis is that they are performed under static conditions, on samples of plasma or enriched platelet suspensions [4]. In contrast with these static tests, bleeding or thrombotic complications occur in whole blood flowing through damaged vessels. Thus, current tests applied to the evaluation of hemostasis provide a fragmented view of the isolated components of the hemostasis, disregarding the interactions that must necessarily occur in flowing blood. Studies using perfusion annular and parallel chamber technologies with circulating blood have contributed significantly to the knowledge on the function of platelets in the hemostatic mechanism and the thrombotic complications under shear conditions [5,6]. More recently developed microfluidic devices have facilitated the implementation of perfusion assays in a more simplified way than the classic approaches, using small blood samples and facilitating the evaluation of the results [1–3,7].

Therefore, the study of blood flow biorheology is of great interest for a better understanding of hemostasis and the effects of antithrombotic drugs [8,9]. Now microfluidics and micro biomimetic flow chambers can provide platforms for the ex vivo study of the effects of flow upon blood coagulation and fibrin formation [10–12].

Due to the introduction of direct oral anticoagulants (DOACs) to circumvent the frequent monitoring and dose adjustment with classic Vitamin K antagonists (VKAs), there is now a need for methods to measure the anticoagulant effects of these drugs in several situations: Hospitalized or critically ill or bleeding patients. Uncertainties about the use of DOACs in patients requiring an urgent invasive procedure, suspicion of overdose, recurrence of thrombotic events or confirmation of adherence, need to be addressed [13,14]. Assessment of the impact of anticoagulant therapies is simple for VKAs, but very complex for the DOACs. Monitoring antiplatelet therapy or assessing the potential risk of bleeding or thrombosis requires specialized equipment, specific devices and a definition of cut-off values for each drug. Unfortunately, tests used to assess the effects of DOACs on coagulation are drug-specific, and not routinely available at clinical labs. Availability of reliable point of care (POC) tests which require less volume of sample and a short turnaround of results would facilitate the evaluation of the anticoagulant activity, the identification of specific patient groups and the guidance of reversal agents in case of overdose.

Moreover, antiplatelet agents are prescribed and administered at fixed doses to patients at risk of cardiovascular complications. Although regular monitoring of their actions is not advised, several studies have demonstrated that responses to antiplatelet drugs are not uniform [15]. There are subgroups of patients in whom different laboratory tests indicate suboptimal responses to antiplatelet drugs. This condition, initially defined as "resistance" to the antiplatelet agent, has evolved to a more descriptive concept of patients with "high on-treatment platelet reactivity" (HPR) [16]. HPR exposes patients to an increased risk of major adverse cardiovascular events, and may require dual therapy. Conversely, the concept "low on-treatment platelet reactivity" (LPR) defines subgroups of patients exposed to an enhanced bleeding risk. Optimized antiplatelet therapy based upon a reliable functional assay will improve the balance of efficacy vs. safety in subgroups of patients.

The combination of techniques evaluating the platelet and coagulation elements of hemostasis is the initial step towards the development of POC devices that could efficiently and reliably evaluate the contribution of both components in minute blood samples or at patients' bedsides, which is highly desirable.

The research work presented here leads to a fundamental contribution to the understanding of hemostasis processes inside vessels, which is of utmost importance to the medical community in order to enhance the treatment of cardiovascular diseases. The design and the validation of the microflow chamber as a tool to characterize a dominant behavior of plasma poor in platelets (PPP) or plasma rich in platelets (PRP) is the base for a highly reliable point-of-care device for antithrombotic treatment monitoring. In the past few years, direct oral anticoagulants (DOACs) were introduced to circumvent the frequent monitoring of classical ones, and therefore decrease the burden on public health systems in countries where the growth of the elderly population has spread the cardiovascular disease impact.

But there is a need to measure the effectiveness of these treatments, especially near the patient. The use of biomimetic microfluidic channels for studying the hemostasis process reduces the time and the number of samples required, and provides a tool to provide results near the patient.

2. Materials and Methods

2.1. Microflow Chamber Design and Manufacturing

The microfluidic device has three main parts: A polydimethylsiloxane (PDMS) part that contains an open microfluidic channel, and it has been manufactured by conventional lithography methods, with a glass-cover to mimic the vasculature tissue and a 3D-printed frame, see Figure 1b. The goal of the printed frame is to apply pressure on the glass in order to seal the channel. Two springs that are embedded in the frame (Figure 1c) allow the exchange of the glass to morphologically characterize the thrombi after the tests.

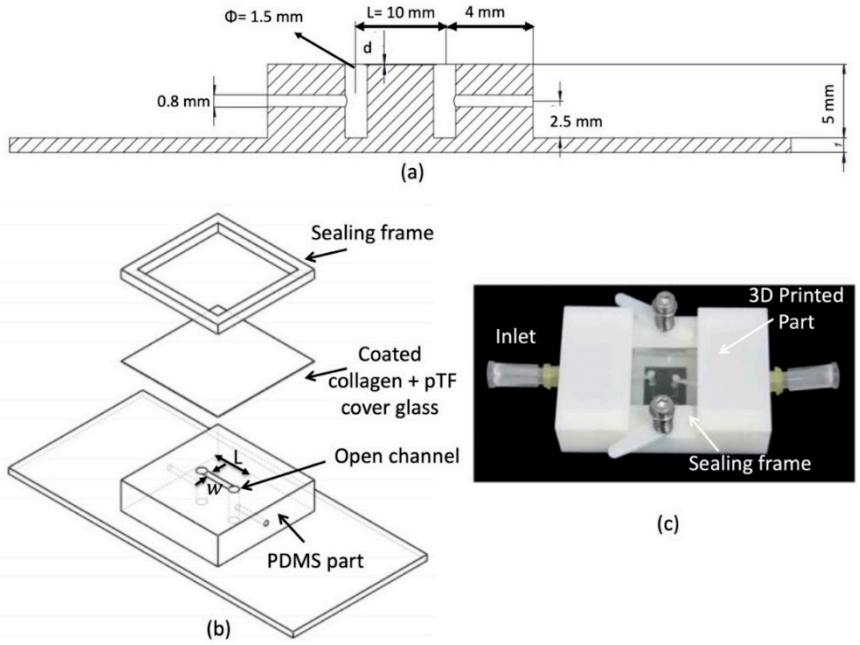

Figure 1. 3D schematics and the picture of the biomimetic microfluidic channel. (**a**) the cross-sectional view of the microfluidic channel. (**b**) 3D assembly of the different parts of the microfluidic channel. (**c**) Real image of the microfluidic channel.

As shown in Figure 1 the microfluidic PDMS part has a channel (width (w = 500 μm), length (L = 10 mm), depth (d = 50 μm)). Two side channels are made with a 1.5 mm puncher to connect with the inlet and outlet of the device. Finally, the channel is sealed with the glass, which is previously coated with collagen and placenta tissue factor to mimic blood vessel structure.

2.2. Biomimetic Coatings and Sample Preparation

Glass slides (18 mm × 18 mm × 1 mm, from Delta Lab) and interdigitated electrodes (Micrux ED_IDE3-Au) were cleaned and functionalized with collagen and tissue factor. Functionalized slides or electrodes were stored at 4 °C overnight. Once assembled, channels were coated overnight with collagen Type I (Chronology Corp. Havertown, PA, USA) and tissue factor (Innovin, Siemens, Madrid, Spain) to achieve coating concentrations equivalent to 30.9 mg/cm^2 and 0.95 ng/cm^2, respectively, as previously described [17], and were flushed with saline prior to perfusion in order to eliminate the remaining collagen over the surface.

Blood samples were collected from healthy adults (n = 10) after written consent in accordance with the ethics committee from the Hospital Clinic de Barcelona.

Blood was drawn into a syringe prefilled with low molecular weight heparin (LMWH) and centrifuged at 14,000 rpm for 2 min to obtain plasma poor in platelets (PPP) and at 1,000 rpm for 3 min to obtain plasma rich in platelets (PRP). PPP and PRP will be used to study the formation of fibrin and platelets aggregates, respectively.

2.3. Flow Assays

The study of blood or plasma flow in a square microchannel can be analyzed by solving the steady-state Navier-Stokes equation for low Reynolds numbers:

$$\nabla \cdot u = 0. \tag{1}$$

$$\nabla P = \nabla \cdot \tau \tag{2}$$

where u is velocity, P is pressure and τ is the wall shear stress.

The wall shear stress can determine the growth rate of the thrombi during the coagulation process, and it is one of the parameters under the study [18]. Blood is stored in a collection tube with anti-coagulants, and then using a centrifuge, the main cells (red blood cells (RBCs) and white blood cells (WBCs)) are separated from the plasma. Plasma constitutes around 55% of the blood volume, and contains numerous proteins, including the clotting factors which are the focus of this study, and other suspended materials. For blood coagulation studies, PRP and PPP are used to evaluate the function of platelets and fibrin(ogen), respectively. While whole blood behaves as a non-Newtonian fluid, and the viscosity changes with the applied shear rate, plasma with a water content of almost 95% behaves as a Newtonian Fluid.

For Newtonian fluids, the shear stress is linearly proportional to the shear rate $\dot{\gamma}$, and the shear rate tensor can be expressed as $\overline{\overline{\tau}} = \eta \cdot \overline{\overline{\dot{\gamma}}}$, being that η is the viscosity of the fluid. Using the relation between the flow rate Q in a rectangular microchannel and the Pressure loss [19]

$$\mathrm{Q} \approx \frac{wd^3}{12\eta L} \nabla P \left[1 - 0.63 \frac{d}{w} \right] \tag{3}$$

where w is the width of the channel, d is the depth and L the length.

Then the wall shear rate $\dot{\gamma}$ can be related to the volumetric flow rate Q according to [20]:

$$\dot{\gamma} \approx \frac{32\, Q}{\pi\, D_h^3} \tag{4}$$

where $D_h = 2w \cdot d/(w + d)$ is the hydraulic diameter of the rectangular channel. Since plasma behaves approximately as a Newtonian fluid, a wall shear rate $\dot{\gamma}$ of 300 s^{-1} was achieved on the glass surface, applying a flow rate of 0.1 mL/h to the microchannel through a syringe pump.

2.4. Image Capture and Analysis

The perfused channels were fixed with paraformaldehyde 1% for 15 min at 4 °C and further incubated with glycine 1% for 10 min to reduce high background staining due to free unreactive aldehyde groups. Then the channels were blocked with 1% bovine serum albumin (BSA) for 15 min prior to incubating with specific antibodies. A combination of indirect and direct immune-fluorescence was carried out as follows.

First, platelets were stained with a mouse anti-CD36 primary antibody for 1 h at room temperature (RT, 37 °C) in a humidified chamber. Then, a secondary antibody anti-mouse Alexa Fluor 488 was incubated together with a conjugated antibody anti-fibrinogen Alexa Fluor 594 for 1 h at RT in a humidified chamber. Pictures were acquired using a confocal microscope (SP5, Leica Microsystems,

Barcelona, Spain). Acquired images from the channels of the micro-chamber were analyzed using the ImageJ software (v 1.43m), (Rasband, W.S., ImageJ, National Institutes of Health, Bethesda, MD, USA).

Co-distributions between the platelets (green) and fibrin (red) were analyzed. The intensity of each marker was densitometrically analyzed individually in each picture, superposed and expressed as a percentage of the covered surface corresponding to the entire image.

2.5. Impedance Characterization

Electrochemical Impedance Spectroscopy (EIS) studies the system response to a small amplitude sinusoidal signal at different frequencies, and it can give information about the analytic molecules in a fluidic solution (for instance, a blood sample). In this new chamber, the glass slide was replaced by the glass with printed electrodes (ED_IDE3-Au) from Micrux (Oviedo, Spain), see Figure 2.

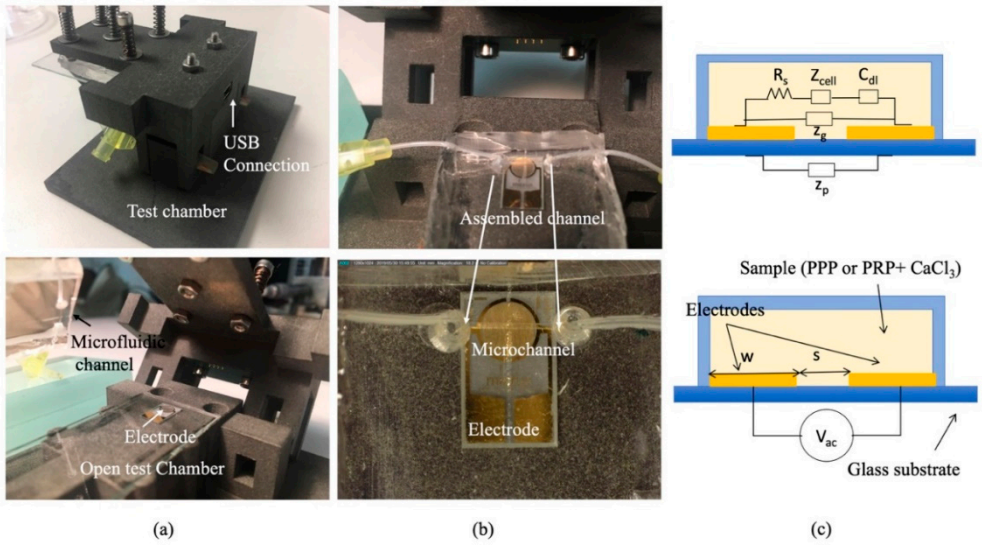

Figure 2. (**a**) Pictures of the test chamber assembled and open. (**b**) Pictures of the microfluidic channel inside the test chamber with the thrombogenic surface with embedded electrodes. (**c**) Impedance model of the electrode inside the channel.

Figure 2a,b show different images of the biomimetic microfluidic channel for impedance measurements. Now the glass cover of the channel has the electrodes (ED_IDE3-Au) from Micrux which are 180 gold strips separated 5 µm apart and with 5 µm in width, forming a 3.5 mm circle. The electrodes close the channel and are biomimetically covered, as described in Section 2.2. Figure 2c portrays the schematics of the electric equivalent circuit of the electrodes. When the plasma with the platelets (PRP—plasma rich in platelets) or fibrinogen (PPP—plasma poor in platelets) flows on the surface of the electrodes, the sensor can be used to determine the composition of the fluidic solution, since their components show a different imaginary and real impedance response at different frequencies. For an arbitrary electrode, its impedance (Z_E) can be described by different components according to [21]:

$$Z_E = (R_s + 2Z_{dl}) \left\| \left(\frac{1}{j\omega C_g} \right) \right\| Z_p \quad (5)$$

where R_s is the resistance of the solution, $Z_{dl} = (R_{ct} + Z_w) \| \left(\frac{1}{j\omega C_{dl}} \right)$ is the double-layer impedance and C_g is the dielectric capacitance and Z_p the parasitic capacitance of the substrate.

The resistance of the solution, $R_s = g/(\sigma W)$, relates to the geometry of the electrode $g = g(L, S)$, where L is the length of the electrode and S the separation between electrodes and the conductivity of the solution σ. In our design, W, the width of the electrode in-plane, and g, are constant parameters of the electrode.

Therefore, R_s is related to the conductivity of the solution, $\sigma = qn_i\left(\mu_p + \mu_n\right)$, where q is the electric charge, μ_p and μ_n are the ionic mobilities of the dominant positive and negative ions in the solution, and n_i is the ionic concentration, which can vary during coagulation.

The double-layer impedance (Z_{dl}) captures the phenomena around the electrode; the term R_{ct} captures the charge transfer between electrodes and Z_w the mass-transfer between them. In case of non-faradaic electrodes, since there is no surface reactions ($Rct \rightarrow \infty$), therefore, there is no mass transfer. Besides, $Z_w \approx 0$, $Z_{dl} = \left(\frac{1}{j\omega C_{dl}}\right)$, where C_{dl} originates from the adsorbed charge layer and diffuse layer charge. For electrode separation higher than Debye length ($\lambda \sim 1$ µm), C_{dl} can be described by diffuse layer capacitance $C_{dl} = C_{dif} = A\sqrt{\frac{2\varepsilon n_i q^2}{kT}}\cosh\left(\frac{q\,V_{ac}}{2kT}\right)$, where A is the area of the electrode (A = wL), V_{ac} is the voltage applied, q is the electric charge, k is the Boltzmann constant, T is the temperature of the solution, and ε is the permittivity of the medium separating the electrodes.

For a parallel plate system, the geometric capacitance form by the electrodes and the solution is $C_g = A\,\varepsilon/S$, where A is the area of the electrodes, ε the permittivity of the medium separating the electrodes and S is the separation between the electrodes.

If the substrate is highly resistive, such as glass (low dielectric constant), the frequency response of an ideal non-Faradaic shows three different regions:

1. For low frequencies $f_{low} = \frac{2}{2\pi R_s C_{dl}}$, C_{dl} dominates the impedance measured.
2. For frequencies $f_{low} < f < f_{high} = \frac{2}{2\pi R_s C_g}$, R_s is the dominant impedance.
3. For frequencies $f > f_{high}$, C_g is the dominant impedance.

The time dependence of the different components is:

R_s is depending upon the concentration of the ions in the solution, since during coagulation different ions are involved. R_s will change during the coagulation process; basically, if the concentration is increased, the conductivity will increase and R_s decreases.

C_{dl} will also increase if the concentration of ions is increased, and finally, the C_g is independent on the ion concentration. C_g changes could be related to changes in the permittivity of the solution, that could change if there were volume changes of the sample, but since our system is inflow, the volume covering the electrodes is constant.

Therefore, as the blood clot is forming, the change in ion species will be detectable using impedance, and the combination of this quantification method with the biomimetic microfluidic chamber allows a quantification of the effects of the shear rate of the process of clot formation.

To study this change of impedance, PalmSens 4 EIS was connected to the electrodes to measure impedance at different frequencies, see USB connection in Figure 2. A 100 µL PPP or PRP sample is loaded to an Eppendorf and withdrawn with a syringe pump.

Prior to each test, the plasma (PPP or PRP) was placed at room temperature for 30 min. Then, the plasma sample was mixed with 1 µL calcium chloride ($CaCl_2$ (5mM)) to induce coagulation. Electrical impedance across the electrodes between 10 Hz and 1 MHz was measured while a sinusoidal voltage of 250 mV was applied.

Illustration of the electrodes in contact with the sample and a photograph of the microfluidic chip is shown in Figure 2.

3. Results

3.1. Flow Assay Results

Figure 3 provides a representative image of the results of microfluidic studies of whole blood with different doses of APLIX and the generated distribution of platelets and fibrin on the perfused surface. The right panel shows bar diagrams representing the proportions of platelet aggregates in green and fibrin masses in red interacting with the collagen/tissue factor surface, as evaluated following the procedure mentioned in Section 2.4. To evaluate the effects of APIX samples with different APIX doses

where tested, see Table 1. Bar graphs in the right of Figure 3 quantify the percentages of the total surface exposed that are covered platelets and fibrin platelet, respectively.

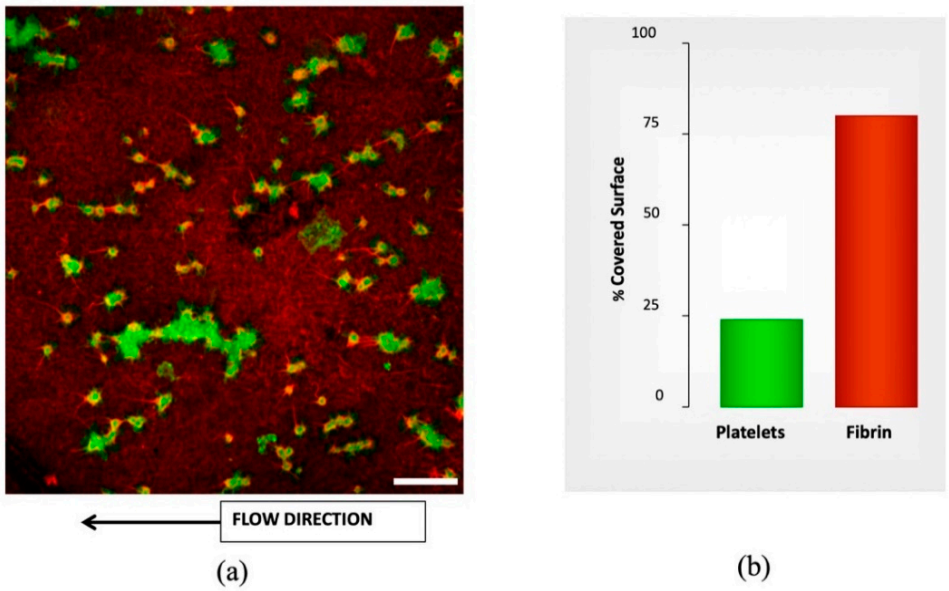

Figure 3. Confocal image labeled by immunofluorescence for morphometric analysis from microfluidic studies. (**a**) Confocal image showing platelets labeled byanti-CD36 Alexa Fluor 488 and Fibrin labeled by anti-fibrin(ogen) Alexa Fluor 594. The thrombogenic surface is a biomimetic combination with type-I fibrillar collagen (30.9 mg/cm^2) and tissue factor (0.95 ng/cm^2). Scale bar = 20 µm. (**b**) The plot shows the quantification of platelet aggregates (green) and fibrin masses (red) interacting with the collagen/tissue factor surface. The bar graphs in the right panel summarize the results as percentages of the total surface exposed.

Incubations with different APIX doses caused dose-dependent decreases in platelet and fibrin surface, reaching levels of statistical significance at 160 ng/mL (* $p < 0.05$ vs. control without APIX and # $p < 0.05$ vs. APIX 10 ng/mL), see Table 1. Microfluidics studies with recalcified citrated blood show similar results with conventional methods at the same shear rate. Table 1 summarizes the percentages of the covered surface.

Table 1. Percentage of the covered surface at shear rate 600 s^{-1}.

[APIX] ng/mL	Platelets	Fibrin
0	23.0 ± 3.0	43.4 ± 4.8
10	17.9 ± 0.9	42.1 ± 1.9
40	14.0 ± 5.3	23.4 ± 7.7
160	5.4 ± 2.2 *#	14.1 ± 4.9 *#

3.2. *Impedance Spectroscopy Assay Results*

The impedance behavior of the clotting process on PRP and PPP that was studied using a 100 µL of the sample flowing on the coated electrode as follows is differentiated and repeatable. Figure 4 shows a different trend for both samples PRP and PPP. Supplementary material shows different repetitions of the same experiment with other samples and the same behavior. Since PPP creates a complete coverage on the electrodes, it affects equally the real and imaginary parts of the impedance detected. PRP contains a high concentration of platelets creating aggregates during coagulation, see Figure 3 (green dots). Therefore, the main change is focalized on the real part of the impedance.

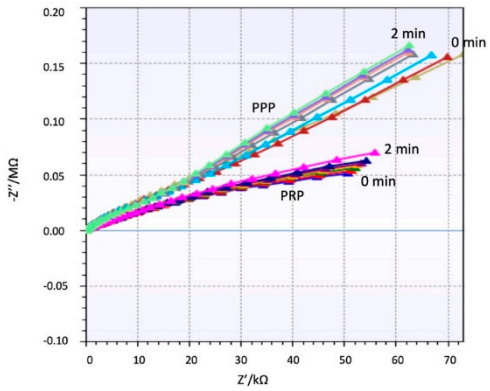

Figure 4. Real and Imaginary part of Impedance for plasma poor in platelets (PPP) and plasma rich in platelets (PRP) over time.

During clotting the coating of the electrodes is changed, modifying the permittivity layer between the electrodes. In the case of PPP, fibrin formation is uniform on the electrodes, and when the coverage is full, the influence on the solution conductivity changes are reduced. For PRP, the coverage of electrodes is not uniform, since the thrombus is always located on certain points, therefore the changes on conductivity are not relevant; consequently, the variations near the electrode cause a noticeable change on the real part, while the imaginary part slightly changes.

The spectrum shows a general capacitive behavior at low frequencies (C_{dl} dominates). The impedance is high at low frequencies and decreases gradually. Around 10^5 Hz, the impedance decreases to the behavior of becoming more resistive (R_s dominates). Both samples PPP and PRP show the same trend, but the impedance of PRP is always higher due to the increased amount of cellular component which increases the resistivity of the solution, especially when $CaCl_2$ is added. Figure 5 shows a clear effect of the coagulation on the impedance modulus during the coagulation process, which results in an increase of impedance. This increase is remarkable for low and high frequencies in PRP samples, while in PPP samples the impedance increases at frequencies higher than 10^5 Hz.

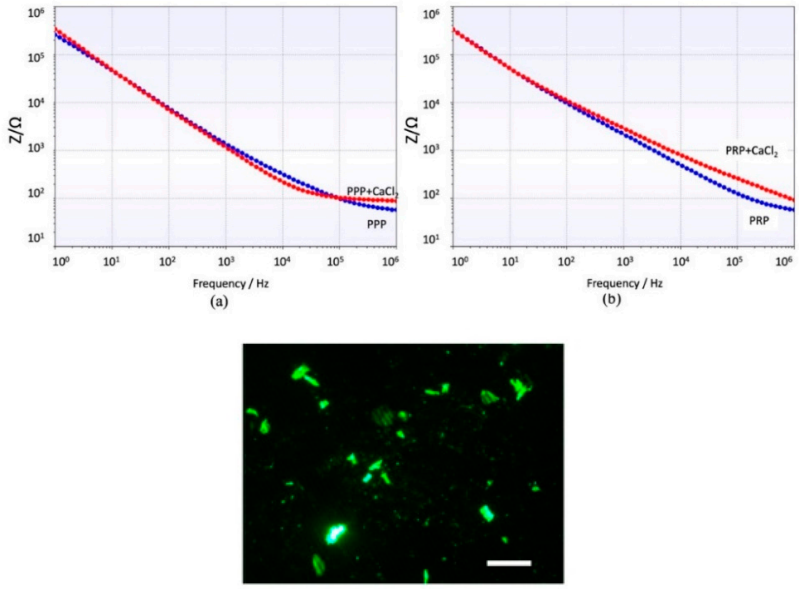

(**c**)

Figure 5. Impedance module at different frequencies after 90 s interaction of the electrode with (**a**) PPP and PPP + $CaCl_2$. (**b**) PRP and PRP + $CaCl_2$. (**c**) Image of the platelets attached on the electrodes. Scale bar = 10 μm.

4. Discussion

Previous studies proved the importance of studying on hemostasis underflow conditions for a better understanding of the process, and nowadays microfluidics technology provides a perfect platform to study this phenomenon. Most of these studies have focused on a global understanding of whole blood behavior during the coagulation process.

New oral anticoagulants (NOACs) used in patients with more complex treatment cases require close monitoring and assessment of the cross-reaction with classic Vitamin K antagonists (VKAs). Hemostasis is a complex process which at least has a double side contribution from platelets and fibrin(ogen). Conventional evaluation methods use an important amount of reagent and sample, and they are time-consuming. However, the introduction of microfabrication techniques has allowed the replica of vein models and biomimetic surfaces to study the complexity of the coagulation process in biomimetic environments [11,22,23] with a reduced amount of reagents.

These biomimetic approaches still require the use of further biomolecular techniques to quantify the presence and quantity of thrombi or clots. Therefore, the techniques are not compatible with near-patient monitoring strategies. Impedance spectroscopy has successfully been applied to monitor the growth of bacteria colonies in biofilm formation [24–26]. The behavior can be extrapolated to the PPP effect that creates a complete coverage on the electrodes similar to biofilm growth, and it affects equally to the real and imaginary part of the impedance detected, as shown in Figure 4.

PRP contains a high concentration of platelets creating aggregates during coagulation, and during this process the electrolytes in solution change and affect the impedance. Previous studies focusing on electrolytes on the solution [27,28] show a different behavior on the real and imaginary part of the impedance, and besides this, a change depending on the concentration of this electrolytes. PRP samples have shown an important influence of the electrolytes in solution and the attachment of the thrombi at the same time, showing a completely differentiated behavior to PPP samples.

The differentiated behavior of PPP and PRP would allow the monitoring of responses to antiplatelet agents present in the samples, while still being able to assess the impact of anticoagulant therapies on the different elements of hemostasis. As for sample volumes, the proposed devices work with a reduced 100 µL sample, and the microfluidics and electronics can be miniaturized in a point of care (POC) system. Besides, the turnaround results are shortened, facilitating a rapid evaluation of the anticoagulant activity, the identification of specific patient groups, and the guidance of reversal agents in case of overdose.

The combination of both analyses (PPP and PRP) in a miniaturized POC device with impedance measurements can evaluate the contribution of platelets and the coagulation mechanism in minute blood samples at patients´ bedsides.

5. Conclusions

The present study has combined microfluidics with impedance spectroscopy to diagnose and control coagulation disorders in a biomimetic approach. The proposed device uses a new micro-manufactured microflow chamber with interchangeable biomimetic surfaces to measure coagulation. Evaluation of the impact on coagulation in minute samples (100 µL) spiked with a new oral anticoagulant APIXABAN (APIX) has been performed using this technique and compared to previous conventional techniques. Both tests show an excellent agreement.

The biomimetic surfaces can be imprinted with gold electrodes, adding the capability to quantify the presence of platelets aggregates or fibrinogen formation from a reduced amount of sample and reagents, and also a minimized time for testing.

Different impedance behaviors of plasma poor in platelets (PPP) and plasma rich in platelets (PRP) has been observed. PPP changes during coagulation are more noticeable at higher frequencies and modify both real and imaginary parts of the impedance. PRP changes are remarkable even at low frequencies, but only at the real part of the impedance. This study is the base for a point-of-care device

capable of quantifying in a short time and near the patient the effect of anticoagulant on fibrinogen formation or platelet aggregation.

Supplementary Materials: The following are available online at http://www.mdpi.com/2072-666X/10/8/534/s1, Figures S1 and S2: Real and Imaginary part of Impedance for different samples of PPP and PRP over the time.

Author Contributions: The conceptualization of the devices was done by G.E., J.C.-T. and J.F.-L. Methodology, testing and validation were done by S.K. and E.M. Writing and reviewing the article was done by J.C.-T. and G.E.

Funding: This was partially supported by the Health Institute Carlos III (ISCIII): Health Technological Development project grant number DTS16/00133 from the Spanish Government together with the European regional development Funds (FEDER) and the Spanish Ministry of Economy and Competitivity, grant nos. CTQ2016-77936-R (funding also from FEDER) and CTQ2017-84966-C2-1-R.

Conflicts of Interest: The authors declare no conflict of interest.

References

1. Neeves, K.B.; Onasoga, A.A.; Wufsus, A.R. The use of microfluidics in hemostasis: Clinical diagnostics and biomimetic models of vascular injury. *Curr. Opin. Hematol.* **2013**, *20*, 417–423. [CrossRef] [PubMed]
2. Shen, F.; Kastrup, C.J.; Liu, Y.; Ismagilov, R.F. Threshold Response of Initiation of Blood Coagulation by Tissue Factor in Patterned Microfluidic Capillaries Is Controlled by Shear Rate. *Arterioscler. Thromb. Vasc. Biol.* **2008**, *28*, 2035–2041. [CrossRef] [PubMed]
3. Li, M.; Ku, D.N.; Forest, C.R. Microfluidic system for simultaneous optical measurement of platelet aggregation at multiple shear rates in whole blood. *Lab Chip* **2012**, *12*, 1355. [CrossRef] [PubMed]
4. Michelson, A.D. Methods for the measurement of platelet function. *Am. J. Cardiol.* **2009**, *103*, 20A–26A. [CrossRef] [PubMed]
5. Sakariassen, K.S.; Houdijk, W.P.; Sixma, J.J.; Aarts, P.A.; de Groot, P.G. A perfusion chamber developed to investigate platelet interaction in flowing blood with human vessel wall cells, their extracellular matrix, and purified components. *J. Lab Clin. Med.* **1983**, *102*, 522–535. [PubMed]
6. Escolar, G.; Mazzara, R.; Castillo, R.; Ordinas, A. The role of the Baumgartner technique in transfusion medicine: Research and clinical applications. *Transfusion* **1994**, *34*, 542–549. [CrossRef]
7. Nagy, M.; Heemskerk, J.W.; Swieringa, F. Use of microfluidics to assess the platelet-based control of coagulation. *Platelets* **2017**, *28*, 441–448. [CrossRef] [PubMed]
8. Onasoga-Jarvis, A.A.; Leiderman, K.; Fogelson, A.L.; Wang, M.; Manco-Johnson, M.J.; Di Paola, J.A.; Neeves, K.B. The Effect of Factor VIII Deficiencies and Replacement and Bypass Therapies on Thrombus Formation under Venous Flow Conditions in Microfluidic and Computational Models. *PLoS ONE* **2013**, *8*, e78732. [CrossRef]
9. Fedosov, D.A.; Dao, M.; Karniadakis, G.E.; Suresh, S. Computational Biorheology of Human Blood Flow in Health and Disease. *Ann. Biomed. Eng.* **2014**, *42*, 368–387. [CrossRef]
10. Jain, A.; van der Meer, A.D.; Papa, A.L.; Barrile, R.; Lai, A.; Schlechter, B.L.; Otieno, M.A.; Louden, C.S.; Hamilton, G.A.; Frelinger, A.L.; et al. Assessment of whole blood thrombosis in a microfluidic device lined by fixed human endothelium. *Biomed. Microdevices* **2016**, *18*, 73. [CrossRef]
11. Zhang, Y.S.; Davoudi, F.; Walch, P.; Manbachi, A.; Luo, X.; Dell'Erba, V.; Miri, A.K.; Albadawi, H.; Arneri, A.; Wang, X.; et al. Bioprinted thrombosis-on-a-chip. *Lab Chip* **2016**, *16*, 4097–4105. [CrossRef] [PubMed]
12. Jain, A.; Graveline, A.; Waterhouse, A.; Vernet, A.; Flaumenhaft, R.; Ingber, D.E. A shear gradient-activated microfluidic device for automated monitoring of whole blood haemostasis and platelet function. *Nat. Commun.* **2016**, *7*, 10176. [CrossRef] [PubMed]
13. Patel, M.R.; Hellkamp, A.S.; Fox, K.A. Point-of-Care Warfarin Monitoring in the ROCKET AF Trial. *N. Engl. J. Med.* **2016**, *374*, 785–788. [CrossRef] [PubMed]
14. Hori, M.; Ohashi, Y.; Pan, G.; Kato, M.; Kajikawa, M. Point-of-Care Device for Warfarin Monitoring Used in the J-ROCKET AF Study. *Circ. J.* **2016**, *80*, 1488–1490. [PubMed]
15. Cattaneo, M. Resistance to antiplatelet drugs: Molecular mechanisms and laboratory detection. *J. Thromb. Haemost.* **2007**, *5*, 230–237. [CrossRef] [PubMed]
16. Lenk, E.; Spannagl, M. Platelet Function Testing—Guided Antiplatelet Therapy. *EJIFCC* **2014**, *24*, 90.

17. Lopez-Vilchez, I.; Tonda, R.; Hernandez, R.M.; Navalon, F.; Diaz-Ricart, M.; Galan, A.M.; Escolar, G. Relative contributions of collagen and tissue factor to thrombus formation on damaged vascular vessels: In-vitro studies with circulating blood. *Coron. Artery Dis.* **2009**, *20*, 392–399. [CrossRef] [PubMed]
18. Papaioannou, T.G.; Stefanadis, C. Vascular Wall shear stress: Basic principles and Methods. *Hell. J. Cardiol* **2005**, *46*, 9–15.
19. Bruus, H. *Theoretical Microfluidics*; Oxford university press: College Park, MD, USA, 2008; Volume 18, p. 363.
20. Yeom, E.; Kang, Y.J.; Lee, S.J. Changes in velocity profile according to blood viscosity in a microchannel. *Biomicrofluidics* **2014**, *8*, 034110. [CrossRef]
21. Dak, P.; Ebrahimi, A.; Alam, M.A. Non-Faradaic Impedance Characterization of an Evaporating Droplet for Microfluidic and Biosensing Applications. *Lab Chip* **2015**, *14*, 2469–2479. [CrossRef]
22. Ting, L.; Feghhi, S.; Karchin, A.; Tooley, W.; White, N.J. Clot-On-A-Chip: A Microfluidic Device to Study Platelet Aggregation and Contractility Under Shear. *Blood* **2013**, *122*, 2363.
23. Lam, W.A. Thrombosis-on-a-Chip: A New Way to Model a Complex Process. *Blood* **2017**, *130*, SCI-10.
24. Mallén-Alberdi, M.; Vigués, N.; Mas, J.; Fernández-Sánchez, C.; Baldi, A. Impedance spectral fingerprint of E. coli cells on interdigitated electrodes: A new approach for label free and selective detection. *Sens. Bio-Sens. Res.* **2016**, *7*, 100–106. [CrossRef]
25. Van Duuren, J.B.; Müsken, M.; Karge, B.; Tomasch, J.; Wittmann, C.; Häussler, S.; Brönstrup, M. Use of Single-Frequency Impedance Spectroscopy to Characterize the Growth Dynamics of Biofilm Formation in Pseudomonas aeruginosa. *Sci. Rep.* **2017**, *7*, 5223. [CrossRef] [PubMed]
26. Clausen, C.; Dimaki, M.; Bertelsen, C.; Skands, G.; Rodriguez-Trujillo, R.; Thomsen, J.; Svendsen, W. Bacteria Detection and Differentiation Using Impedance Flow Cytometry. *Sensors (Basel)* **2018**, *18*, 3496. [CrossRef] [PubMed]
27. Eldarrat, A.; High, A.; Kale, G. Influence of sodium chloride content in electrolyte solution on electrochemical impedance measurements of human dentin. *Dent. Res. J. (Isfahan)* **2017**, *14*, 25–31. [CrossRef]
28. Boumya, W.; Laghrib, F.; Lahrich, S.; Farahi, A.; Achak, M.; Bakasse, M.; El Mhammedi, M.A. Electrochemical impedance spectroscopy measurements for determination of derivatized aldehydes in several matrices. *Heliyon* **2017**, *3*, e00392. [CrossRef] [PubMed]

Biofabrication

International Society for Biofabrication

Cost-effective microfabrication of sub-micron-depth channels by femto-laser anti-stiction texturing

To cite this article before publication: Shadi Karimi *et al* 2019 *Biofabrication* in press https://doi.org/10.1088/1758-5090/ab6665

IOP Publishing Journal Title
Journal **XX** (XXXX) XXXXXX https://doi.org/XXXX/XXXX

Cost-effective microfabrication of sub-micron-depth channels by Femto-laser anti-stiction texturing

Shadi Karimi[1], Pouya Mehrdel[1], Jasmina Casals-Terré[1], Josep Farré-Llados[1]

[1] Mechanical, Fluids and Aerospace Engineering, Universidad Politécnica de Cataluña, Terrassa, Barcelona, Spain

E-mail: josep.farre.llados@upc.edu

Received xxxxxx
Accepted for publication xxxxxx
Published xxxxxx

Abstract

Micro Electro Mechanical Systems (MEMS) and microfluidic devices have found numerous applications in the industrial sector. However, they require a fast, cost-effective and reliable manufacturing process in order to compete with the conventional methods. Particularly, at the sub-micron scale, the manufacturing od devices are limited by the dimensional complexity. A proper bonding and stiction prevention of these sub-micron channels are two of the main challenges faced during the fabrication process of low aspect ratio channels. Especially, in case of using flexible materials such as polydimethylsiloxane (PDMS). This study presents a direct laser microfabrication method of sub-micron channels using an infrared (IR) ultrashort pulse (femtoseconds) capable of manufacturing extremely low aspect ratio channels. These microchannels are manufactured and tested varying their depth from 0.5 µm to 2 µm and width of 15, 20, 25, and 30 µm. The roughness of each pattern was measured by an interferometric microscope. Additionally, the static contact angle of each depth was studied to evaluate the influence of femtosecond laser fabrication method on the wettability of the glass substrate. PDMS, which is a biocompatible polymer, was used to provide a watertight property to the sub-micron channels and also to assist the assembly of external microfluidic hose connections. A 750nm depth watertight channel was built using this methodology and successfully used as a blood plasma separator (BPS).
The device was able to achieve 100% pure plasma without stiction of the PDMS layer to the sub-micron channel within an adequate time. This method provides a novel manufacturing approach useful for various applications such as point-of-care devices.

Keywords: Femtolaser, Biofabrication, Microfluidic, Blood/plasma separation

1. Introduction

The fast improvement of MEMS and microfluidics during the last decade has allowed the development of new research areas [1][2]. Currently, this research has consolidated on new devices that require cost-effective and reliable manufacturing processes. Rapid prototyping is an important stage in the fabrication of these systems, enabling fast verification of designs without the need for microfluidic simulations that do not always prove to be accurate enough [3]. For these applications, there are many materials and manufacturing methods such as photo sensible resins (SU-8) and polymers (PDMS) which are shaped by conventional soft lithography or

selective laser sintering printers [4]-[9]. PDMS is one of the most used polymers for its excellent optical properties and compatibility with different microfluidics and biological applications, however, its low Young modulus can produce a collapse of the structure at low aspect ratios. Glass is another candidate but the hose connections can not be easily integrated. For diagnostic applications, there is a need to achieve low aspect ratio channels which can be connected easily to external pipes. Structuring adequately the surface of the glass can allow the combination of both materials for low aspect ratio structures and facilitating the fabrication of biocompatible applications.

Blood is classified as connective tissue and is composed of two elements: plasma and blood cells. Plasma is essentially an aqueous solution and constitutes around 55% of the blood volume. Blood cells are Red Blood Cells (RBCs), White Blood Cells (WBCs), and platelets. Plasma is the base of a wide range of assays and is needed at clinical chemistry testing for prognosis [8]. To this end, there is a need for a low cost and reliable method to produce blood plasma filters that can separate plasma from a single droplet of blood. Previous researchers have focused on low aspect ratio channels to achieve filtration using wet chemical etching on the glass [10][11]. This method is based on extremely aggressive chemicals with a huge environmental impact and difficult to industrialize. Therefore, there is a manufacturing limitation to provide cost-effective and reliable method channels with a characteristic height lower than 1.5 µm for blood-plasma filtering. RBCs are biconcave, measuring approximately 6 to 8 µm in diameter and a thickness at the thickest point of 2 to 2.5 µm and a minimum thickness in the center of 0.8 to 1 µm, being much smaller than most other human cells which under high shear flows the shape of the red blood cells can deform [12] reducing its smaller dimension even to less than 1 µm. Consequently, channels with less than one micron in depth are required to achieve a reliable filtration rate and also it is necessary to avoid high shear stress to prevent cell fragmentation.

There are a large portfolio of manufacturing methods to produce channel dimension in micron-scale [13]-[15], however, at the sub-micron range, the manufacturing processes are more complex [16] and limited, especially if watertight channels are required [17]. Focusing on watertight channels, Chen et. al [18] presented a fabrication method using PDMS that took advantages of simplicity and low cost although the material deformed easily. Turning this disadvantage into an advantage, Park et.al [19] studied the PDMS collapse related to the ratio of width and depth of the original micro-channel to form sub-micron channels afterward. Reactive Ion Etching (RIE) is a well-known manufacturing method capable to manufacture from 40-nm to 300-µm-depth channels on different base materials such as glass [20] or PDMS [21] but limited to cleanroom facilities. Laser beam machining (LBM) is a growing non-traditional machining process where laser thermal energy is used to remove material from metallic or non-metallic surfaces [22]. Different laser source wavelengths are used to machine infrared (IR) and ultraviolet (UV) wavelengths range. CO_2 IR lasers are the most widely used and more cost-effective compared to UV although when it is used on some polymeric materials the temperature of the laser not only reduces the precision but also changes the material properties. This technology has been used in micron range to produce through holes which requires assembly to achieve the whole microfluidic device, such as Hao-Bing et al. [23] where the channel shape was defined using CO_2 laser on a precured film.

Other authors used Polymethylmethacrylate (PMMA) and pressure-sensitive adhesives [3][24][25] but the range of channel thickness was always limited to the micron range and bonding was more complex, therefore different materials were required [24] or different laser passes [26]. From the other hand controlling the wettability of the surface is important for various practical applications. For instance, hydrophilic surfaces are useful for capillary behavior in microfluidic channels while hydrophobic surfaces are good for self-cleaning of contaminations. However, hydrophobic surfaces are difficult to bond. As glass substrates are useful for various applications, we study the controlled modification of characterized surface wettability with femtosecond laser passes [25].

UV laser sources energy concentration is high and can generate a smaller focus spot size in sub-micron level, but the range of materials is limited. Matthew et al. [27] used UV laser ablation to machine micron-sized channel on biocompatible polymers, however further thermal bonding was required. IR femtosecond laser technology joints the wide range of materials with precision. Nowadays, IR laser sources (i.e. ytterbium) with ultrashort pulses opens the possibility to achieve high precision. Ultra-short-pulse lasers can machine substrates at the wavelength where they are usually transparent. This provides a precision down to the tenth of nanometers without affecting the nearby area [28]. Researchers implemented this technology with a directly fully enclosed channel [29] in the micron range, and it is being introduced in the industry to drill high-aspect-ratio holes.

This manuscript presents a laser direct microfabrication method that uses IR femtosecond laser pulses to produce anti-stiction [30] extremely low aspect ratio sub-micron channels on a glass substrate. At atmospheric conditions, different channel depths has been manufactured from 500 nm to 2µm. The sub-micron channel is sealed by a PDMS layer via Oxygen-plasma to enable the watertight behavior without the need of any other step or layer.

A BPS is manufactured by this method to filter the cellular component of blood and achieves 100% pure plasma from undiluted blood. This method improves the reproducibility on

the size and the shape from the method presented by Park et.al [19] which is faster and easier than RIE [20][21]. Importantly, the stiction of the PDMS layer either during the manufacturing process or during the operation [27] is avoided due to the texture and roughness of the laser machined surface of the glass. To confirm if surface wettability is a function of surface morphology, surface roughness is measured and the regime is studied between two well-known wetting theories by Wenzel [31] and Cassi-Baxter [32].

2. Materials and method

Firstly the potential of femtosecond laser micromachine for rapid prototyping of microfluidic channels on the surface of glass substrates was assessed. To validate the femtosecond laser manufacturing accuracy in the sub-micron range, a template with different channels was designed. Each channel was formed by two parallel rectangular blocks to investigate the in-plane accuracy. The distance between the two blocks (channel width) is the same as the width of the block. Different channel depth was studied, modified H parameter from 500 nm to 2 µm as shown in Figure 1. This figure shows the details of dimension W that characterizes these columns which vary from 15 µm to 30 µm. These rectangular cross-section microchannels were fabricated by performing different laser passes for each depth with the same laser power.

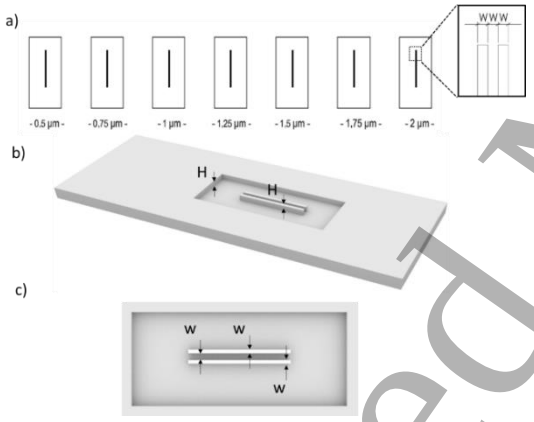

Figure 1: (a) 2D view of the seven different Template in depth (H) from the range of 0.5µm (Nanochannels) to 2µm (microchannels). Each template fabricated in four different channel width (w): 15µm, 20 µm, 25 µm, and 30 µm. (b) the 3-D view schematic of one template. (c) the top view of the template.

After studying the influence of different patterns and different height on the glass, the desired sketch was carved to develop a blood plasma filtering device. This pattern is a reservoir with an array of pillars which not only holds the weight of PDMS on the top but also conduct the extracted plasma in the reservoir to the plasma collector channels as it is shown in Figure 2.

To manufacture the desired shape and depth on the glass, the femtosecond laser works as an engraving machine using a laser spot of approximately 10 µm, with the power of 20W, and pulse duration of approximately 350fs. The femtoseconds laser is controlled by a CNC system and depending on the depth different passes are required on the surface. Each laser pass is 120º tilt from its previous to ensure the maximum uniformity at the engraving area. First laser pass made 0.5-µm-depth and after that for each laser pass, 0.25-µm-depth is used. Therefore, for the channel of 2 µm depth, the laser performs 7 passes.

Surface roughness has a strong effect on wettability of a surface and the contact angle. The effect of roughness changes if the droplet wets the surface grooves or if air pockets are left between the droplet and the surface. Two different theories were developed to explain the effect of surface roughness on wettability. If the surface is wetted homogeneously, the droplet is in Wenzel [31] state. In Wenzel state, adding surface roughness will enhance the wettability caused by the chemistry of the surface. This model predicts enhanced hydrophilicity for hydrophilic surfaces and an enhanced hydrophobicity for hydrophobic surfaces. This model takes into account a complete wetting of droplet with the underneath substrate. If the surface is wetted heterogeneously, the droplet is in Cassie-Baxter [32] state. This model assumes that the liquid does not completely wet the roughened substrate. The Cassie-Baxter model predicts that roughening a surface always increases the contact angle. If a surface is rough enough so that air may be entrapped between the liquid and the solid, the interface becomes composite and the contact angle increases with roughness even if the surface chemistry is intrinsically hydrophilic. The most stable contact angle can be connected to the Young contact angle. The contact angles calculated from the Wenzel and Cassie-Baxter equations are

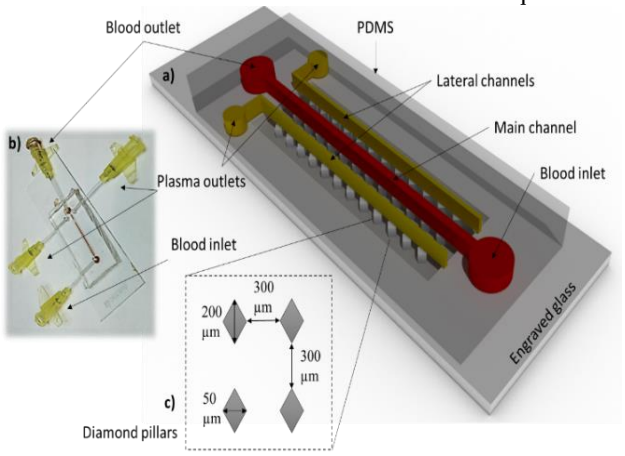

Figure 2: (a) Schematic of the BPS device which contains a PDMS block on the top part and an engraved glass by laser on the bottom part. (b) a picture of the real device. (c) The pattern that is carved on the glass with the dimensions of the array of diamond pillars.

good approximations of the most stable contact angles with real surfaces.

The obtained nano and microchannels were measured using a confocal microscope model Sensofar PLU neox with a 10XDI objective to evaluate the accuracy on the sub-micron range depth. Furthermore, the surface roughness was evaluated using an optical zoom 4X in an area of 317.06 x 237.38 μm^2. The channel template of Figure 1a was manufactured three times. This template contains four different width columns (15 µm, 20 µm, 25 µm, and 30 µm) that form a channel between them with the same dimension, see drawing dimension W at the detail of Figure 1.

In order to investigate the influence of the roughness generated by the femtosecond laser irradiation on surface wettability, the measurement of the static contact angle of each template was carried out using an optical video contact angle system (OCA software, SCA20 module, Dataphysics). To perform the test, a 0.7 µL droplet of de-ionized water 25º, having a surface tension of 71.99±0.05 mN/m, was dispensed on the samples using a 500-µL Hamilton syringe unit. The static contact angle based on the Young-Laplace fitting was measured using the sessile drop method with dedicated software.

2.1. Device Fabrication

The device is conceived in two parts: A PDMS layer where the microchannels and the external connection are located in a glass holder that has the sub-micron reservoir pattern. Figure 3 shows the three steps of the manufacturing process. Step A includes a conventional soft lithography process to make a mold. The pattern of the microchannels on the PDMS is engraved by this mold. Besides, the syringe pump is connected through the external connection on the PDMS. Step B uses femtoseconds laser pulses to define the low-aspect-ratio pillar shapes and the sub-micron channel walls on the glass. for this manner firstly, a 2D model of the sub-micron channel was defined using AutoCAD 2018 as shown in Figure 2c. The model with Rhinoceros was edited to define the regions to manufacture the micro-channel of a certain depth. A

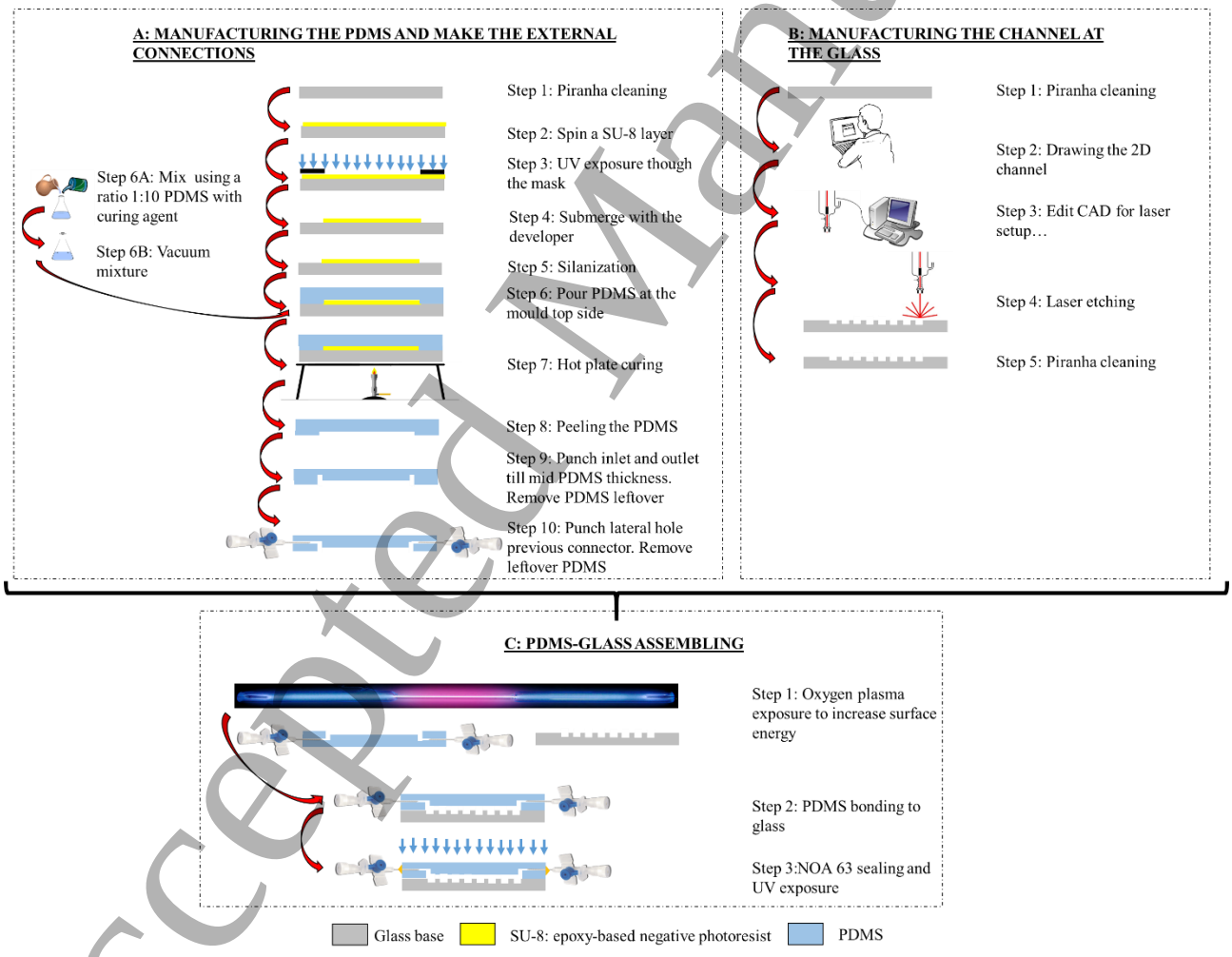

Figure 3: Manufacturing method steps. A is the manufacturing method of the micro-channels on a PDMS base. B is the nanochannels manufacturing method on a glass base. C is the bonding process that has a watertight channel.

femtosecond laser model AgieCharmilles LASER P 400 U was used. The sub microchannel was cleaned using sonication and immersion in a Piranha solution as following:

First: sonication using acetone for 15min and rinsing with distilled water.

Second: 20min in Piranha (1:3 H2O2:H2SO4) and rinsing with distilled water and dry on the hot plate at 95ºC for 10 minutes right before the PDMS-Glass bonding process starts.

In step C the PDMS is bonded to the glass via Oxygen plasma. In order to ensue the hose connections are sealed completely, Norland Optical Adhesive 63 (NOA63) is used. This adhesive is a clear, colorless, liquid photopolymer that will cure via UV light exposure.

2.2. Blood plasma separator (BPS)

In order to validate the fabricated sub-micron pillars, a BPS system was designed and manufactured as an application. The BPS contains two parts; the bottom part is a glass which carved by laser in depth of 0.75 µm and contains an array of diamond pillars in order to hold the weight of the top part which is a PDMS block. The PDMS has three separated channels, one main channel in the middle of two lateral channels. The main channel is filled by the blood sample and two collector channels are designed to collect the extracted plasma by capillary force. The PDMS and the glass were bonded via Oxygen plasma. The PBS device was placed under an optical upright microscope (Dino-Lite Digital Microscope Edge Series USB Cameras).

The blood samples that are used in the BPS were collected from healthy volunteers from Banc de Sang i Teixits de Catalunya.. The samples were stored in a vacutainer collection tube which contains anti-coagulant (Ethylenediamine tetra-acetic acid) to postpone the coagulation phenomena during the experimental setup. To maximize the livability of the cellular components, the samples were stored at 4 ºC temperature and were gently mixed back and forward to prevent possible undesirable cell sedimentation prior to testing. All the experiments were processed at the room temperature (20-25 °C).

The blood sample was injected from the blood inlet using a syringe pump at a flow rate of 10 ml/min. The height of the pillars is 0.75 µm to prevent entrance of red blood cells at the plasma collector channel even at high shear forces. Then pure plasma was driven to the plasma reservoir and blood with a higher concentration of red blood cells was drawn from blood outlet.

To evaluate the quality of the plasma and the performance of the sub-micron filter, the plasma purity parameter was measured. An image processing was developed by an open-source ImageJ software to analyze the particles by their population. To determine the purity of the extracted plasma, a rectangular area (200 µm × 400 µm) in the blood inlet was selected and compared with the same size area in the plasma outlet. These areas were captured by microscope after the plasma collector channels were filled completely. The number of blood cells in these areas were counted by the particle analysis method of the ImageJ software. The plasma purity evaluates the number of red blood cells ratio at the plasma outlets compared to the initial red blood cells at the inlet according to equation 1.

$$Purity\% = \left(1 - \left(\frac{final\ cells\ density}{initial\ cells\ density}\right)\right) * 100\% \quad (1)$$

3. Results & discussion

3.1. Sub-micron channels manufacturing method

During the manufacturing process, the laser is focused on the material surface that absorbs the energy and transforms it into the gaseous state to generate the sub-micron channel. For extremely low depth 0.5 µm, the ablation of the surface may not be complete and, according to Figure 4a, some protruding peaks appear. Figure 4b shows a cross-section of the manufactured part and in this figure. For 0.5- µm –depth channels, the material ablation is not completed or some ablated material is deposited and bonded again at the surface forming some protruding peaks. These peaks avoid the achievement of a flat surface and prevent a complete seal with the PDMS cover. Figure 4 clearly shows the pattern of the

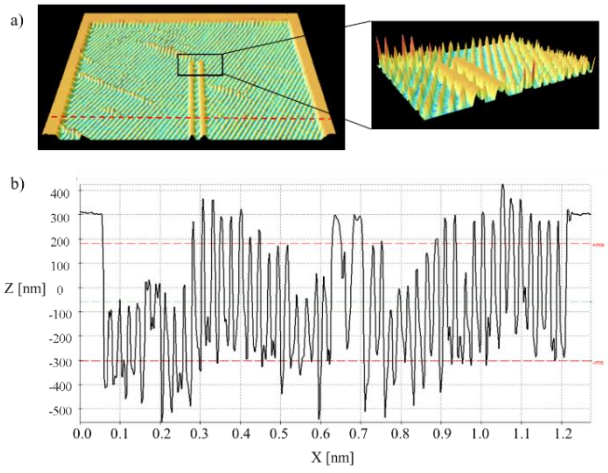

Figure 4: 0.25-µm-width and 0.-5µm-depth channel template measurement using a confocal microscope. (a) shows the 3D view of the region treated with the laser that contains some protruding regions. Redline is the cross-section position is shown in (b). The cross-section shows the protruding regions are higher in depth than the level of the original surface.

laser machining direction for 0.5-µm-depth channels while in 0.75-µm-depth channels template this pattern disappears as shown in Figure 5. This is due to the fact that two laser passes were performed to define the depth. Furthermore, the protruding peaks disappear as well, see Figure 5 and more roughness is generated on the surface.

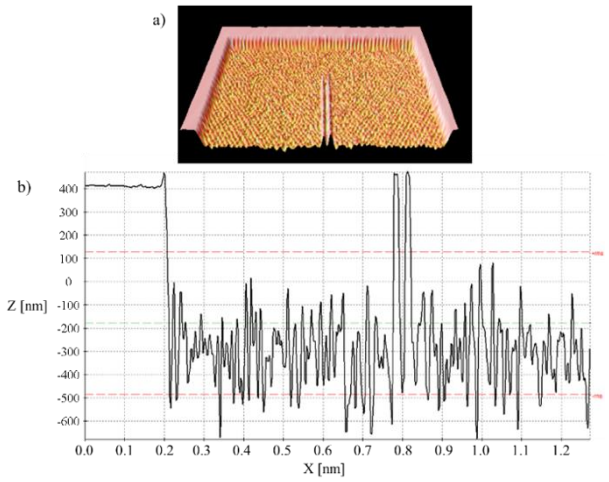

Figure 5: Channel template of 0.75 µm depth and 15µm width measurement using a confocal microscope

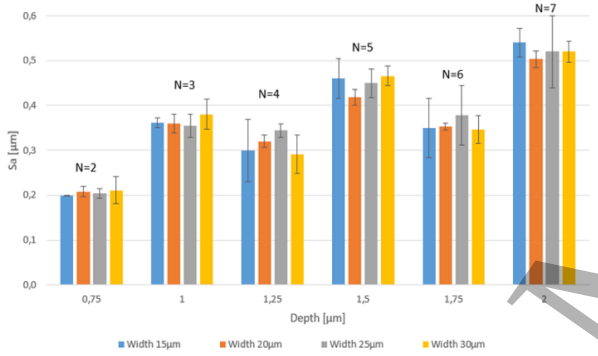

Figure 6: Confocal surface roughness (Sa) measurements from 0.75 µm to 2 µm depth channel template with a different width. It expresses, as an absolute value, the difference in height of each point compared to the arithmetical mean of the surface. N is the number of laser passes.

Figure 6 shows that there is no influence of the channel width on the roughness and outlines that the roughness increases as the depth of the channel increases, which means the number of laser passes increases. Additionally, when the number of laser passes is an odd number (the case of 1-µm, 1.5-µm, and 2-µm-depth template) the roughness presents a maximum and at even number (the case of 0.75-µm, 1.25-µm, 1.75-µm depth template) the roughness improves. This is due to the second laser pass which improves the roughness that the previous laser pass pattern.

As shown in Figure 7, the width of the channel has higher accuracy when the channel width and depth are lower. Results also denote that channel depth has a higher influence on accuracy. For channels with less than 1µm-depth, the deviation is between 0.4% and the deviation reaches 7% when the channel width increases. The accuracy regarding the depth increases with it reaching a maximum of 10% deviation for the 2 µm-depth channels. As it is mentioned before, to achieve higher depth, the number of laser passes increases. This fact has a certain effect on the distance between the columns defined. This distance increases 550 nm ± 100 nm at each laser pass from the designed dimensions. This accuracy is one order of magnitude higher than in conventional soft lithography. However, the depth of the channels is unachievable by soft lithography. On the other hand, when the channel depth increases, the channel width increases as well, therefore, lowering the precision, but being still similar to the soft lithography process. For wider channels, the accuracy of the laser decreases exponentially as shown in Figure 8. This figure shows the case of the template of 30 µm width and 0.75 µm-depth, where the deviation is 1.54 µm and this deviation increases with the depth reaching a 4.31 µm deviation for the template of 2 µm-depth. As it is expected, the width of the column has the opposite behavior, as the depth of the channel increases the column becomes narrower and the channel width

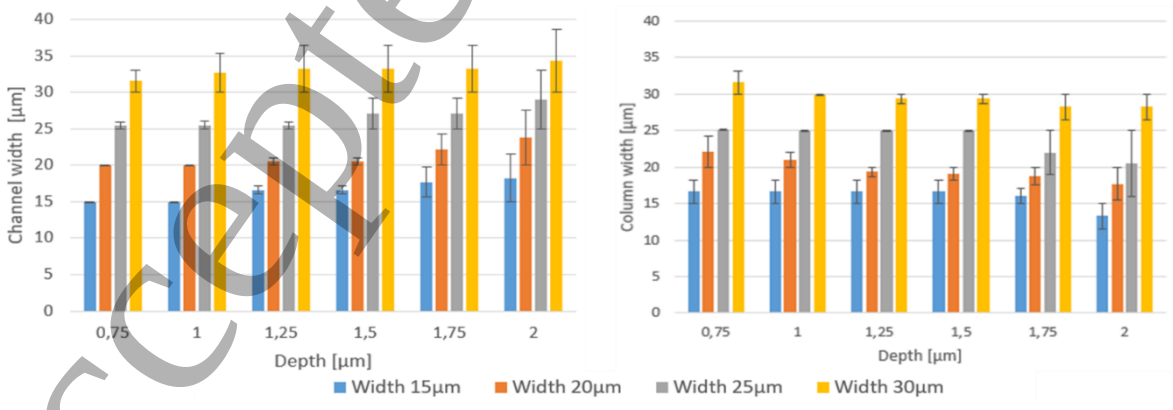

Figure 7: Confocal 3D measurement of the channel width and the column width at the channel template depth 0.75 µm, 1 µm, 1.25 µm, 1.5 µm, 1.75 µm, and 2 µm.

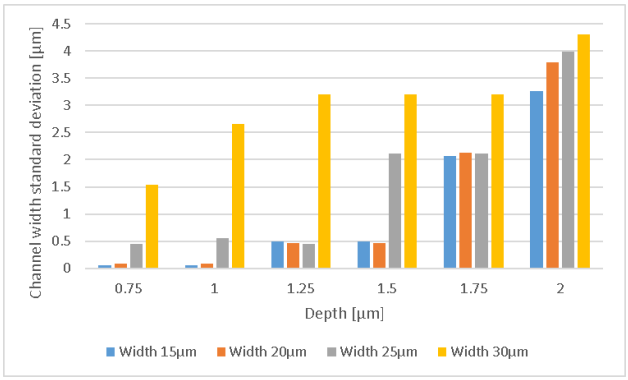

Figure 8: Channel width standard deviation at depth of 0.75, 1, 1.25, 1.5, 1.75, and 2 µm.

increases. When the channel depth is low, the width of the column is in an average of a 10% wider than the designed dimensions and as the channel depth increases this tendency decrease; for the case of 2 µm-depth channels, the width of the column is in an average of a 3.6% narrower than the designed dimensions.

The angle of contact between pure water and a perfectly clean glass is 0°and for ordinary water increase from 8° to 18°. Figure 9a shows the static contact angle on glass samples irradiated at laser pass of 2, 3, 4, 5, 6, and 7, revealing a hydrophilic behavior for all the different laser passes but show a dependence of the wettability on the laser passes employed. As shown in Figure 9b the measured contact angle is 11°, since dionized water is used on a slide of glass.

This actual behavior can be explained assuming that the texture generated during the laser machining, trap air between the water and the glass substrate below, preventing a complete wetting of the substrate. Interferometry images of Figure 4a and Figure 5a show the cross-section of the profile shape, characterized by laser groove and peaks. The dimension of the grooves does not appear to change significantly, confirming that the contact angle measurements depend mostly on surface texture rather than the roughness.

According to the contact angles measurements as shown in Figure 9 on the sub-micron range, the channel is completely hydrophilic to perform self-driven fluid test [10] and useful for the blood plasma separator applications.

3.2. Blood plasma separator Application

Figure 10 shows the schematic of the top view of the BPS device and also the microscopic picture of the channels. Blood was injected from the inlet and flew through the main channel as shown in Figure 10. Afterward, the plasma was spread through the bottom part. Since the height of the pillars was less than the minimum size of RBCs, all the cells were trapped in the main channel. The pure plasma in the bottom part was

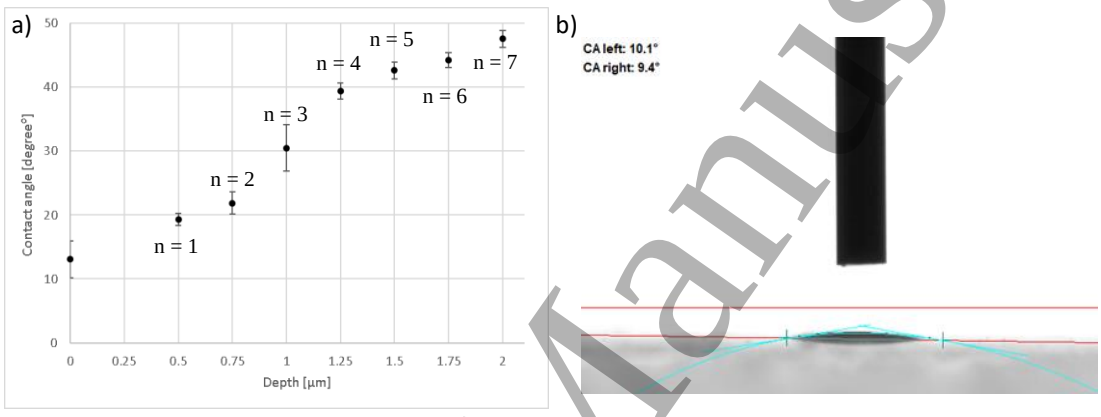

Figure 9: (a)Contact angles measurements at the template depth of 0.5 µm, 0.75 µm, 1 µm, 1.25 µm, 1.5 µm, 1.75 µm, 2 µm. Zero is on the surface of the glass. (b)Microscopic picture of the contact angle measurement of a 0.7 µl of DI water on the glass template depth of 0 µm.

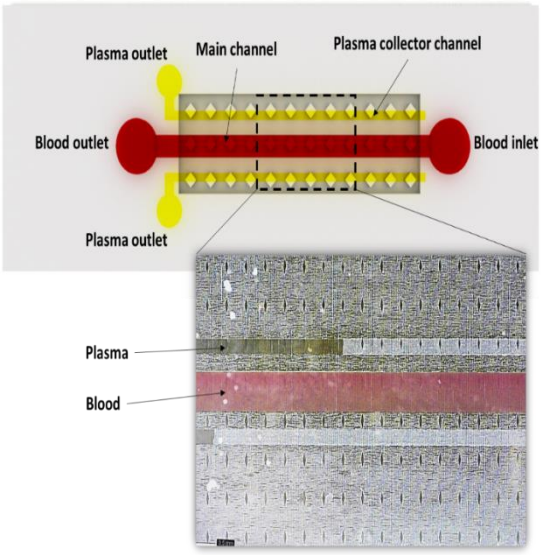

Figure 10: The schematic of BPS device from the top view and the microscopic view of the BPS right after the blood injection.

filled in two lateral channels by the capillary. Figure 10 also shows the filling process of plasma into the lateral channels. After directly counting the number of blood cells in blood inlet and plasma outlets, by the help of ImageJ software, it has been confirmed that final blood cells in the plasma collector channels were zero. Since no cell could penetrate to the lateral channel, the purity of the extracted plasma according to equation 1 was obtained 100%. The excellent purity of the extracted plasma is the significant advantage of this BPS. This figure also denotes the high transparency of the BPS that allows analyzing the calorimetry and particle counting.

4. Conclusion

A novel method to manufacture a watertight sub-micron channel has been developed and tested. The open-top sub-micron channels with an array of pillars were manufactured using a femtosecond laser and the watertight property was reached by a PDMS cover. The femtosecond laser has been evaluated to manufacture sub-micron channels above 500nm. The applicability of the manufactured sub-micron channels have been validated in a BPS device. Plasma was successfully extracted from blood with the highest efficiency of 100%. This method has several advantages compared to current sub-micron watertight manufacturing methods:

- It is a rapid manufacturing method for channel dimension greater than 750 nm in depth. (about 40 seconds for a rectangles with the area of 18.5*12.5 mm^2)
- The PDMS is not sticking to the sub-micron channel either during the bonding fabrication or operating the device due to the texture of the surface.
- The number of laser passes has a significant influence on the pattern. The odd number of laser pass increases the roughness while the next laser pass decreases the roughness.
- The number of laser passes has an influence on the contact angles: as the laser passes increase, the surface wettability decreases.
- The channel width precision decreases when increasing the channel width and depth.
- Laser focus spot size limits the decrease of the width of the sub-micron channel.
- The glass maintains good transparency and enables colorimetric and particle counts analysis systems.

Acknowledgments

This work is partially supported by Microrelleus, S.L (www.microrelleus.com) and the Spanish Ministry of Economy and Competitivity, grant nos. CTQ2016-77936-R (funding also from FEDER) and CTQ2017-84966-C2-1-R. Special acknowledgment to Raúl García from Microrelleus, S.L for his support on the laser manufacturing.

References

[1] **Yanazawa, H. and Homma, K., 2017** Growing market of MEMS and technology development in process and tools specialized to MEMS. In 2017 IEEE Electron Devices Technology and Manufacturing Conference (EDTM) (pp. 143-144). IEEE.

[2] **Laermer, F., 2018** MEMS at Bosch—Invented for life. In 2018 IEEE Micro Electro Mechanical Systems (MEMS) (pp. 237-240). IEEE.

[3] **De Marco, C., Eaton, S. M., Suriano, R., Turri, S., Levi, M., Ramponi, R., ... & Osellame, R. 2010** Surface properties of femtosecond laser ablated PMMA. ACS applied materials & interfaces, 2(8), 2377-2384.

[4] **Yoon, Y., Lee, J., Ra, M., Gwon, H., Lee, S., Kim, M.Y., Yoo, K.C., Sul, O., Kim, C.G., Kim, W.Y. and Park, J.G., 2019** Continuous Separation of Circulating Tumor Cells from Whole Blood Using a Slanted Weir Microfluidic Device. Cancers, 11(2), p.200.

[5] **Patel, J.N., Gray, B.L., Kaminska, B., Wu, N.C. and Gates, B.D., 2013** SU-8-and PDMS-based hybrid fabrication technology for combination of permanently bonded flexible and rigid features on a single device. Journal of Micromechanics and Microengineering, 23(6), p.065029.

[6] **Mehrdel, P., Karimi, S., Farré-Lladós, J. and Casals-Terré, J., 2018** Novel Variable Radius Spiral–Shaped Micromixer: From Numerical Analysis to Experimental Validation. Micromachines, 9(11), p.552.

[7] **Chhina, S.K., Perez, C.F. and Parameswaran, M., 2012** Microfluidic system to detect DNA amplicons using agglutination technique. Journal of Micromechanics and Microengineering, 22(11), p.115038.

[8] **Farré-Lladós, J., Westerberg, L.G. and Casals-Terré, J., 2017** New method for lubricating wind turbine pitch gears using embedded micro-nozzles. Journal of mechanical science and technology, 31(2), pp.797-806.

[9] **Mackenzie, M.D. and Kar, A.K., 2019** Microfluidic devices and biological lasers for biophotonic applications. In Journal of Physics: Conference Series (Vol. 1151, No. 1, p. 012001). IOP Publishing.

[10] **Madadi, H., Casals-Terré, J., Castilla-López, R. and Sureda-Anfres, M., 2014** High-throughput microcapillary pump with efficient integrated low aspect ratio micropillars. Microfluidics and nanofluidics, 17(1), pp.115-130.

[11] **Madadi, H., Casals-Terré, J. and Mohammadi, M., 2015** Self-driven filter-based blood plasma separator microfluidic chip for point-of-care testing. Biofabrication, 7(2), p.025007.

[12] **Sutera, S.P. and Mehrjardi, M.H., 1975** Deformation and fragmentation of human red blood cells in turbulent shear flow. Biophysical journal, 15(1), pp.1-10.

[13] **Trotta, G., Volpe, A., Ancona, A. and Fassi, I., 2018** Flexible micro manufacturing platform for the fabrication of PMMA microfluidic devices. Journal of Manufacturing Processes, 35, pp.107-117.

[14] **Chen, L., Wen, J., Zhang, P., Yu, B., Chen, C., Ma, T., Lu, X., Kim, S.H. and Qian, L., 2018** Nanomanufacturing of silicon surface with a single atomic layer precision via mechanochemical reactions. Nature communications, 9(1), p.1542.

[15] **Karimi, S., Farré-Lladós, J., Mir, E., Escolar, G. and Casals-Terré, J., 2019** Hemostasis-On-a-Chip: Impedance Spectroscopy Meets Microfluidics for Hemostasis Evaluation. *Micromachines*, *10*(8), p.534.

[16] **Chan, Y.C., Lee, Y.K. and Zohar, Y., 2006** High-throughput design and fabrication of an integrated microsystem with high aspect-ratio sub-micron pillar arrays for free-solution micro capillary electrophoresis. Journal of micromechanics and microengineering, 16(4), p.699.

[17] **Wu, Z., Yan, H., Chen, H. and Huang, H., 2009** One-stage fabrication of sub-micron hydrophilic microchannels on PDMS. Applied Surface Science, 255(8), pp.4702-4704.

[18] **Chen, X. and Zhang, L., 2018** Review in manufacturing methods of nanochannels of bio-nanofluidic chips. Sensors and Actuators B: Chemical, 254, pp.648-659.

[19] **Park, S.M., Huh, Y.S., Craighead, H.G. and Erickson, D., 2009** A method for nanofluidic device prototyping using elastomeric collapse. Proceedings of the National Academy of Sciences, 106(37), pp.15549-15554.

[20] **Bu, M., Melvin, T., Ensell, G.J., Wilkinson, J.S. and Evans, A.G., 2004** A new masking technology for deep glass etching and its microfluidic application. Sensors and Actuators A: Physical, 115(2-3), pp.476-482.

[21] **Garra, J., Long, T., Currie, J., Schneider, T., White, R. and Paranjape, M., 2002** Dry etching of polydimethylsiloxane for microfluidic systems. Journal of Vacuum Science & Technology A: Vacuum, Surfaces, and Films, 20(3), pp.975-982.

[22] **Chryssolouris, G., 2013** Laser machining: theory and practice. Springer Science & Business Media.

[23] **Liu, H.B. and Gong, H.Q., 2009** Templateless prototyping of polydimethylsiloxane microfluidic structures using a pulsed CO2 laser. Journal of Micromechanics and Microengineering, 19(3), p.037002.

[24] **Liu, K., Xiang, J., Ai, Z., Zhang, S., Fang, Y., Chen, T., Zhou, Q., Li, S., Wang, S. and Zhang, N., 2017** PMMA microfluidic chip fabrication using laser ablation and low temperature bonding with OCA film and LOCA. Microsystem Technologies, 23(6), pp.1937-1942.

[25] **Wang, Z.K., Zheng, H.Y., Lim, C.P. and Lam, Y.C., 2009** Polymer hydrophilicity and hydrophobicity induced by femtosecond laser direct irradiation. Applied physics letters, 95(11), p.111110.

[26] **Mohammed, M.I., Quayle, K., Alexander, R., Doeven, E., Nai, R., Haswell, S.J., Kouzani, A.Z. and Gibson, I., 2015** Improved manufacturing quality and bonding of laser machined microfluidic systems. Procedia Technology, 20, pp.219-224.

[27] **Roberts, M.A., Rossier, J.S., Bercier, P. and Girault, H., 1997** UV laser machined polymer substrates for the development of microdiagnostic systems. Analytical chemistry, 69(11), pp.2035-2042.

[28] **Ben-Yakar, A. and Byer, R.L., 2004** Femtosecond laser ablation properties of borosilicate glass. Journal of applied physics, 96(9), pp.5316-5323.

[29] **Jagannadh, V.K., Mackenzie, M.D., Pal, P., Kar, A.K. and Gorthi, S.S., 2014** Imaging flow cytometry with femtosecond laser-micromachined glass microfluidic channels. IEEE Journal of Selected Topics in Quantum Electronics, 21(4), pp.370-375.

[30] **Mastrangelo, C.H., 1999** Suppression of stiction in MEMS. MRS Online Proceedings Library Archive, 605.

[31] **Wenzel, R.N., 1936** Resistance of solid surfaces to wetting by water. Industrial & Engineering Chemistry, 28(8), pp.988-994.

[32] **Cassie, A.B.D. and Baxter, S., 1944** Wettability of porous surfaces. Transactions of the Faraday society, 40, pp.546-551.